Ageing impairs the regenerative capacity of regulatory T cells in central nervous system remyelination

Alerie Guzman de la Fuente[1,2,3*], Marie Dittmer[1], Elise Heesbeen[1,4], Nira de la Vega Gallardo[1], Jessica White[3], Andrew Young[1,5], Tiree McColgan[1], Amy Dashwood[6,7], Katie Mayne[1,8], Sonia Cabeza-Fernández[2,3], John Falconer[1,9], Francisco Javier Rodriguez-Baena[3], Christopher E. McMurran[10,11], Mohammed Innayatullah[12,13], Khalil S. Rawji[14], Robin J.M. Franklin[14], James Dooley[6,7], Adrian Liston[6,7], Rebecca Ingram[1], Vijay K. Tiwari[1,12,13,15], Rosana Penalva[1], Yvonne Dombrowski[1] and Denise C. Fitzgerald[1*]

[1]Wellcome-Wolfson Institute for Experimental Medicine, Queen's University Belfast, Belfast, BT9 7BL, Northern Ireland, UK.

[2]Institute for Health and Biomedical Sciences of Alicante (ISABIAL), Alicante, 03010, Spain.

[3] Instituto de Neurosciencias CSIC-UMH, San Juan de Alicante, 03550, Spain.

[4]Current address: Division of Pharmacology, Institute for Pharmaceutical Sciences, Utrecht University, Utrecht, The Netherlands.

[5] Current address Patrick G Johnston Centre for Cancer Research, Queen's University Belfast, Belfast, BT9 7BL, Northern Ireland, UK

[6] Department of Pathology, University of Cambridge, CB2 1QP, Cambridge, UK

[7] Babraham Institute, CB22 3AT, Cambridge, UK

[8]Current address: Department of Pathology and Laboratory Medicine, University of British Columbia, G227-2211 Wesbrook Mall, Vancouver, BC, V6T 2B5, Canada.

[9]Current address: CRUK Beatson Institute, G61 1BD, Glasgow, UK

[10] Department of Clinical Neurosciences, University of Cambridge, Cambridge, UK

[11]Department of Medical Epidemiology and Biostatistics, Karolinska Institute, Stockholm, Sweden

[12] Institute of Molecular Medicine, University of Southern Denmark, 5000 Odense, Denmark

[13] Danish Institute for Advanced Study (DIAS), 5230 Odense, Denmark

[14] Altos Labs - Cambridge Institute of Science, Granta Park, Cambridge CB21 6GP, UK

31 [15] Department of Clinical Genetics, Odense University Hospital, 5000 Odense, Denmark

32

33

34 *Corresponding authors:

35 Denise C. Fitzgerald, d.fitzgerald@qub.ac.uk

36 Alerie G. de la Fuente, guzman_ale@isabial.es

37

Abstract

Myelin regeneration (remyelination) is essential to prevent neurodegeneration in demyelinating diseases such as Multiple Sclerosis, however, its efficiency declines with age. Regulatory T cells (Treg) recently emerged as critical players in tissue regeneration, including remyelination. However, the effect of ageing on Treg-mediated regenerative processes is poorly understood. Here, we show that expansion of aged Treg does not rescue age-associated remyelination impairment due to an intrinsically diminished capacity of aged Treg to promote oligodendrocyte differentiation and myelination. This decline in regenerative Treg functions can be rescued by a young environment. We identified Melanoma Cell Adhesion Molecule 1 (MCAM1) and Integrin alpha 2 (ITGA2) as novel candidates of Treg-mediated oligodendrocyte differentiation that decrease with age. Our findings demonstrate that ageing limits the neuroregenerative capacity of Treg, likely limiting their remyelinating therapeutic potential in aged patients, and describe two novel mechanisms implicated in Treg-driven remyelination that may be targetable to overcome this limitation.

Introduction

Myelin is critical to the metabolic support and function of axons in the central nervous system (CNS)[1]. CNS myelin is produced by oligodendrocytes and damage to oligodendrocytes or myelin causes neurological impairment[2–4]. Myelin regeneration (remyelination) is highly neuroprotective and holds potential to restore lost function for patients with demyelinating diseases such as Multiple Sclerosis (MS)[5–8]. Like most regenerative processes, remyelination efficiency declines with age[9–11], contributing to age-associated disease progression and the accumulation of irreversible disability[12]. Age-associated remyelination decline has been linked to intrinsic changes in the capacity of oligodendrocyte progenitor cells (OPC) to respond to damage in the aged CNS[13–15], changes in physical properties and the microenvironment (e.g extracellular matrix) of the aged CNS

64 which makes it refractory to remyelination[16,17] and impaired capacity of other cells involved in the
65 process of myelin regeneration (e.g macrophages, microglia, astrocytes) to drive this process [18–23].
66 Despite the critical neuroprotective role of remyelination[8,24], there are currently no approved
67 remyelination-enhancing therapies, a key unmet medical need. Thus, understanding how ageing
68 alters the different cellular mechanisms governing myelin regeneration is key to overcoming age-
69 associated remyelination failure. This holds potential to prevent neuronal loss and the accumulation
70 of irreversible cognitive, sensory and motor disabilities.

71 Regulatory T cells (Treg) have recently emerged as key cellular players in tissue regeneration
72 due to both anti-inflammatory functions and capacity to modulate tissue-resident stem cell
73 differentiation[25,26]. Similar crosstalk has also been described in the CNS, where we and others
74 showed that Treg promote oligodendrocyte progenitor cell (OPC) differentiation and CNS
75 remyelination[27–29]. The discovery of pro-remyelinating functions of Treg opened a new therapeutic
76 avenue to prevent remyelination decline and associated neurodegeneration. However, whether this
77 important neuroregenerative function of Treg is impaired with age remains unknown.
78 Understanding how ageing affects myelin-regenerative functions of Treg is essential to determine
79 the relevance and suitability of potential Treg-based pro-remyelination therapies in patients of
80 advanced age in MS and other demyelinating diseases.

81 Here, we show that ageing impairs the capacity of natural Treg to drive OPC differentiation
82 *in vitro* and myelination *ex vivo*. Surprisingly, this defect was reversible in a young remyelinating
83 environment *in vivo*. Transcriptomic comparison of young and aged Treg identified Melanoma Cell
84 Adhesion Molecule 1 (MCAM1) and Integrin alpha 2 (ITGA2) as novel candidates of Treg-mediated
85 OPC differentiation that decrease with age. This study identifies Treg-driven OPC differentiation as a
86 remyelination mechanism that is impaired by ageing and identifies novel Treg-expressed candidates
87 (ITGA2, MCAM), which enhance OPC differentiation and should be further investigated to determine
88 its potential relevance as therapeutic targets to promote CNS remyelination.

89

90 **Results**

91 **Tissue-resident Treg are increased in the aged CNS**

92 We first examined the frequency of murine Treg with age, and in agreement with previous
93 studies[30,31], found increased numbers and proportions of Treg in aged mice compared to young mice
94 in spleen and blood (**Fig. 1 A-E**). Next, we investigated whether ageing impacted T cell populations in
95 the CNS. As described previously[32–34], we observed an increase in the proportion of $CD8^+$ and $CD4^+$ T
96 cells in aged murine CNS tissue with significant differences observed more prominently in spinal cord
97 than brain (**Sup. Fig. 1A-H**). We also observed a significant increase in the proportion of Treg in the
98 spinal cord (**Fig. 1 F, G**) and a non-significant trend in the brain (**Fig. 1 I, J**). Proportions of tissue-
99 resident ($CD69^+$) Treg[35] were increased both in the aged brain and spinal cord (**Fig. 1 H, K**). Previous
100 studies showed that ageing impairs migration of Treg to damaged muscle[36]. To determine if ageing
101 affects the capacity of Treg to accumulate in demyelinated lesions in the CNS we used two models of
102 demyelination, lysolecithin-induced demyelination, and experimental autoimmune
103 encephalomyelitis (EAE), a model of immune-mediated demyelination. Despite the low frequency of
104 Treg in demyelinated areas, we did not observe any differences in Treg density in either of the two
105 models at the time points investigated (**Fig. 1L-N**). This suggests that aged Treg have a similar
106 capacity to accumulate in demyelinated CNS tissue when compared to young Treg although
107 differences at other phases of CNS damage cannot be conclusively ruled out.

108

109 **Expansion of Treg does not rescue impaired OPC differentiation in aged mice**

110 We next verified that oligodendrocytes numbers were comparable in the young and aged
111 healthy CNS (**Sup. Fig. 2 A-D**)[37,38], but that OPC differentiation into $CC1^+$ oligodendrocytes was
112 impaired in aged demyelinated lesions *in vivo* as previously reported[10,13] (**Sup**. **Fig. 2 E, F**). We next
113 investigated whether expanding Treg populations in aged mice would recover oligodendrocyte
114 differentiation. Administration of IL-2/anti-IL-2 *in vivo* significantly expanded systemic $CD25^+Foxp3^+$
115 Treg (~3-5-fold increase in blood and spleen) (**Fig 2 A-C**) with a trend of higher densities of Treg in

116 demyelinated lesions of Treg-expanded mice (**Sup. Fig. 2 G-J**) which was not statistically significant
117 although numbers were low. We first examined whether Treg expansion enhanced the
118 remyelination response in young mice. As myelin regeneration is highly efficient in young rodents[9,10],
119 and our previous findings showed that Treg accelerated oligodendrocyte differentiation[27], we
120 examined oligodendrocyte differentiation at a comparatively early time point of 7 days-post-lesion
121 (dpl), when OPC differentiation is just starting in this model[39]. While there were no changes in
122 overall $Olig2^+$ cell density, Treg expansion significantly increased the number of $Olig2^+CC1^+$
123 differentiated oligodendrocytes in young mice (**Fig. 2D-F**). Next, we investigated whether Treg
124 expansion accelerate OPC differentiation in aged mice. Taking into account that remyelination is
125 delayed in aged mice, we first examined oligodendrocyte differentiation at 10dpl as a relevant time
126 point at which OPC differentiation has started in aged mice. Contrary to young mice, Treg expansion
127 did not significantly change the density of $Olig2^+$ cells or $Olig2^+CC1^+$ differentiated oligodendrocytes
128 in aged mice at 10dpl (**Fig. 2 G-I**). For a direct comparison to the timepoint in young mice, we also
129 examined oligodendrocyte differentiation at 7dpl in aged mice and observed no differences (data
130 not shown). We also evaluated neurofilament (NFH) and myelin basic protein (MBP) colocalization as
131 a surrogate measure of remyelination. As for OPC differentiation, Treg expansion did not enhance
132 axon wrapping in aged mice (**Fig. 2 J-L**). Hence, we hypothesised that the myelin-regenerative
133 capacity of Treg may be intrinsically impaired in aged Treg, irrespective of Treg population
134 frequency.
135

136 **Aged Treg demonstrate an impaired intrinsic capacity to enhance myelin production**

137 To compare the capacity of young and aged Treg to enhance OPC differentiation and
138 myelination, we first investigated effects on oligodendrocyte development. To do this, we isolated
139 natural Treg from the spleens and lymph nodes of young (3-4 months) and aged (14-18 months)
140 mice (**Sup. Fig. 3 A, B**) and co-cultured these Treg with neonatal murine OPCs. While neither young
141 nor aged Treg modified OPC proliferation *in vitro* (**Fig. 3 A, B**), young Treg significantly increased OPC

142 differentiation into MBP-expressing oligodendrocytes, in agreement with our previous findings of
143 Treg secretome[27,40]. Aged Treg however, did not enhance OPC differentiation demonstrating an
144 impairment in their capacity to support this necessary step in the process of myelin formation (**Fig. 3**
145 **C-E**).

146 To determine if the inability of aged Treg to support OPC differentiation was functionally
147 relevant to the process of myelin production, we compared the capacity of young and aged Treg to
148 drive myelin ensheathment of axons *ex vivo.* To do this, we co-cultured murine organotypic brain
149 slices with young or aged Treg for 7 days. Young Treg significantly enhanced axonal myelination
150 compared to control slices as described before[27]. However, aged Treg failed to significantly increase
151 myelination compared to controls (**Fig. 3 G**). In contrast to our observations in OPC differentiation,
152 we did not detect significant differences between young and aged Treg when evaluating myelination
153 index (**Fig. 3G**) but on balance, these *in vitro* and *ex vivo* data suggest that aged Treg fail to
154 significantly drive myelin production.

155

156 **Myelin-regenerative capacity of aged Treg is restored in a young environment**

157 We previously reported that Treg depletion using diphtheria toxin (DT) in B6.129(Cg)-
158 *Foxp3*$^{tm3(DTR/GFP)Ayr}$/J (FoxP3-DTR)[41] mice impaired OPC differentiation and remyelination, which was
159 rescued by the administration of wild type Treg[27]. Thus, we next compared the regenerative capacity
160 of young and aged Treg in a model of lysolecithin-induced spinal cord myelin damage *in vivo.*
161 Following endogenous GFP^{+} Treg depletion (**Fig. 4 A**, **Sup. Fig. 3 C, D**), we administered wild type
162 (GFP^{-}) young or aged Treg intraperitoneally and confirmed comparable detection of adoptively
163 transferred Treg in each group (**Sup. Fig. 3 E, F**). We next compared the neuroregenerative capacity
164 of adoptively transferred young and aged wild type Treg to enhance OPC differentiation during
165 remyelination (**Fig. 4 A**). We did not observe any differences in the burden of damage for each
166 experimental group, indicated by the lesion area (**Sup. Fig. 3 H**). There was also no difference in the
167 number of oligodendrocyte lineage cells, quantified by Olig2 immunostaining (**Fig. 4 B-D**), or

168 proliferating OPCs (Olig2$^+$Ki67$^+$) at 14 days post-lesion (dpl) (**Sup. Fig. 3 G, I, J**). As before[27], Treg
169 depletion impaired OPC differentiation into CC1$^+$ and ASPA$^+$ oligodendrocytes, which was rescued by
170 adoptive transfer of wild type young Treg. Unexpectedly however, aged Treg injected into young
171 Treg-depleted mice also rescued impaired OPC differentiation, comparably to young Treg, (**Fig. 4 B,**
172 **C, E, F**). To determine if aged Treg not only rescued OPC differentiation but also restored
173 remyelination, we examined axonal wrapping through the quantification of circular MBP$^+$ patterns
174 around NFH$^+$ axons as an early indication of axonal remyelination. Both, young and aged Treg
175 administered to Treg-depleted mice, restored axonal wrapping to levels comparable to non-depleted
176 controls (**Fig. 4 G-J**). These findings suggest that the age-induced defect of neuroregenerative Treg
177 functions observed *in vitro/ex vivo* is reversible in a young systemic environment *in vivo*, and
178 therefore, potentially therapeutically targetable.
179
180 **Young Treg partially rescue OPC differentiation during remyelination in aged mice**
181 Next, we investigated whether young Treg could rescue impaired remyelination in aged mice
182 using Foxp3-DTR mice in which GFP$^-$ young and aged Treg were adoptively transfer following DT-
183 mediated Treg depletion. In contrast to our findings in young Treg-depleted mice, aged mice without
184 Treg showed decreased Olig2$^+$ cell density in the demyelinating area which was not rescued neither
185 by young nor by aged Treg (**Fig. 5 A, B**). As per young mice, Treg depletion did not impair OPC
186 proliferation (**Fig. 5 C**), suggesting that the decrease in Olig2$^+$ cells likely reflects either an impaired
187 survival or migration of oligodendrocyte lineage cells to the damaged area. The decreased density of
188 Olig2$^+$CC1$^+$ oligodendrocytes in the absence of Treg was partially rescued by the transfer of young
189 Treg into these animals but not by transferred aged Treg, which were significantly different to the
190 non-depleted control (**Fig. 5 A, C**). However, it is important to highlight that we did not detect
191 statistically significant differences between aged Treg depleted mice receiving young or aged Treg
192 (**Fig. 5 A, D**) and thus, we interpret these findings with caution. A further reason to be cautious in
193 interpreting these results is that contrary to young recipients, adoptively transferred Treg were not

194 detectable in the classic lymphoid organs (spleen, lymph nodes) of aged Foxp3-DTR mice (**Sup**. **Fig. 4**
195 **E, F**), suggesting that the adoptively transferred cells have a different migration pattern in aged
196 recipients, and thus we cannot be sure that young and aged cells have the same reconstitution
197 capacity or distribution. Additionally, since young and aged Treg failed to restore Olig2^{+} cell density
198 in aged mice (**Fig. 5B)**, the age-associated remyelination impairment, even when Treg are expanded,
199 is associated not only with impaired Treg regenerative capacity but also with a refractory aged CNS
200 environment that may limit OPC responsiveness to Treg-derived cues, as shown for other factors
201 previously[13].
202
203 **Ageing significantly alters Treg transcriptome**
204 We next sought to identify how ageing impairs the myelin regenerative functions of Treg by
205 examining gene expression differences in natural Treg purified from young and aged female mice.
206 RNA sequencing (RNAseq) analysis showed that young and aged Treg clustered separately (**Fig. 6 A,**
207 **C**) as shown in the literature[42,43] and identified 1423 upregulated and 302 downregulated mRNA
208 transcripts in aged Treg compared to young Treg (**Fig. 6 B**). However, there was no difference in the
209 expression of classic Treg markers such as *Foxp3*, *Cd4* or *Il2ra* (**Sup. Fig. 5 B**). Pathway analysis
210 identified that the differentially expressed genes were associated with pathways linked to the
211 adaptive immune response, lymphocyte-mediated immunity, phagocytosis, cell-surface receptor
212 signalling and membrane invagination (**Fig. 6 D)**. Genes that were upregulated with ageing were
213 enriched for the following GO biological processes: extracellular matrix organisation, cell migration,
214 synapse assembly, axonal guidance, cell adhesion and inflammatory and immune responses (**Fig. 6**
215 **E**). On the other hand, mRNA transcripts that were downregulated in aged Treg were associated with
216 defence responses to virus, B cell proliferation and protein folding GO biological processes (**Fig. 6 E)**
217 (GO cellular component, GO Molecular function and Kyoto Encyclopedia of Genes and Genome
218 (KEGG) database pathways analysis is shown in **Sup. Fig. 5**). To identify potential mechanisms
219 underlying how ageing may impair myelin regenerative functions of Treg, we examined expression

220 of genes associated with the Treg tissue repair programme described recently for skin, colon, lung
221 and adipose tisse[44]. Unexpectedly, most of the 31 Treg tissue repair programme hallmark/signature
222 genes[44] were in fact upregulated with ageing, except for *Klrb1, Ccr5, Selplg, Bach2, Rad50, Tfrc, Cd84*
223 *and Cd164* (**Fig. 6 F, G**). No difference in expression was detected in these hallmark genes between
224 male and female natural Treg, showing that sex does not alter the expression of genes associated
225 with the tissue repair programme (**Sup. Fig. 5 C, D**). These data suggest that the mechanism(s)
226 involved in Treg-driven myelin regeneration capacity that are impaired with ageing, are likely
227 different to mechanisms from the Treg tissue repair programme described by Delacher et al[44].
228

229 **Mcam and Itga2 are associated with Treg capacity to drive oligodendrocyte formation**

230 To narrow down age-induced changes in Treg that diminish their capacity to induce OPC
231 differentiation, we first investigated whether the putative mechanisms are soluble or contact-
232 mediated; the latter being suggested by the close physical association of Treg with OPCs observed in
233 co-cultures (**Fig. 7 A**) and in EAE-induced, demyelinated lesions *in vivo* (**Fig. 7 B**). Young natural Treg
234 were co-cultured either directly in contact with OPC, or in the same well but separated using a
235 transwell, which allowed for the exchange of secreted molecules but not direct OPC-Treg contact.
236 While young Treg co-cultured directly with OPCs enhanced OPC differentiation into MBP^+
237 oligodendrocytes, this pro-differentiating effect was lost when Treg were physically separated from
238 OPCs (**Fig. 7 C, D**). To identify potential cell-to-cell contact mechanisms responsible for Treg-driven
239 OPC differentiation that may be lost with ageing, we combined our aged Treg RNA sequencing data
240 with a publicly available RNAseq dataset that compares between OPCs, newly differentiated and
241 differentiated oligodendrocytes[45]. We hypothesised that ligand-receptor interactions between Treg
242 and plasma membrane receptors enriched in OPCs underlie the pro-differentiation effect of Treg on
243 OPC. We prioritised ligand-receptor partnerships between Treg and OPCs that were impacted by
244 ageing, to identify mechanisms that could explain the lost myelin regenerative capacity of aged Treg.
245 We then performed a protein-protein interaction analysis using String[46] (**Fig. 7 F**) and prioritised

246 plasma membrane proteins that had the highest decrease in expression for aged Treg and the
247 highest number of potential binding partners amongst OPC-enriched receptors compared to
248 oligodendrocytes (**Fig. 7 G**). We identified the following key candidates: *Ccr7, Itga2* (CD49b), *Klrb1c*
249 (NK1.1), *Ly6c1, Mcam* (CD146) and *Sell* (CD62L) (**Fig. 5 F-H**). Next, we used a loss-of-function
250 approach to investigate whether these candidates may confer the lost regenerative capacity of aged
251 Treg, namely, CD62L, NK1.1, LY6C, MCAM (CD146) and ITGA2 (CD49b). Of these five targets,
252 antibody-mediated blocking of MCAM (CD146) and ITGA2 (CD49b) on Treg prior to Treg-OPC co-
253 culture inhibited the capacity of young Treg to drive OPC differentiation *in vitro* as indicated by the
254 fold change in the percentage of MBP^+ cells and the MBP^+ area per well (**Fig. 8 A-C, Sup. Fig. 6 A, B**).
255 This suggests that MCAM and ITGA2 are previously unidentified mediators of pro-remyelinating
256 functions of Treg and are downregulated with age.

257 Next, we sought to determine whether MCAM and ITGA2 would directly promote OPC
258 differentiation by treating neonatal OPCs with recombinant ITGA2 and MCAM. While treatment with
259 rMCAM for up to 6 days *in vitro* did not affect OPC proliferation or differentiation (**Sup. Fig. 6C, E-G**),
260 rITGA2 directly enhanced OPC differentiation by day 3 (**Fig. 8 D-G**). rITGA2 did not significantly
261 change the proportion of proliferating OPC (**Sup. Fig. 6 D**) or the proportion of MBP-expressing
262 oligodendrocytes (**Fig. 8 D, E**). However, we observed an increased complexity of oligodendrocyte
263 morphology in rITGA2-treated cultures as indicated by the enhanced number of intersections
264 detected by Sholl analysis on ITGA2-treated OPCs (**Fig. 8 F, G**). This suggests that oligodendrocytes in
265 rITGA2 treated cultures are at later stage of development which aligns with an acceleration of
266 differentiation. Therefore, while rITGA2 directly promoted OPC differentiation, rMCAM did not,
267 suggesting that the function of this latter cell adhesion molecule in Treg-mediated OPC
268 differentiation may be to facilitate OPC-Treg interaction and potentially to activate other pro-
269 differentiative mechanisms rather than itself directly driving OPC differentiation.

270 To determine whether a young environment could boost MCAM and ITGA2 expression by
271 aged Treg, we adoptively transferred young and aged Treg expressing red fluorescent protein (RFP^+)

272 obtained from Foxp3-RFP mice (C57BL/6-*Foxp3*^{tm1Flv}/J Foxp3-IRES-mRFP) into young, Treg-depleted
273 mice and assessed ITGA2 and MCAM expression in spleen and lymph node after 11 days by flow
274 cytometry (**Sup. Fig. 7 A, B**). Due to technical challenges and a lack of further aged FoxP3 reporter
275 mice, only n=2-3 was possible in this study which limits interpretation of statistical significance of
276 our findings. The proportions of MCAM$^+$ or ITGA2$^+$ cells within total Foxp3-RFP$^+$ populations were
277 low in basal conditions and were significantly increased in both aged and young Treg upon adoptive
278 transfer (**Sup. Fig. 7 C, F**). To examine the extent of expression of each marker on a per cell basis, we
279 quantified median fluorescent intensity of MCAM$^+$RFP$^+$ and ITGA2$^+$RFP$^+$ Treg and observed
280 decreased expression of both markers in aged Treg compared to young Treg, in agreement with our
281 RNAseq findings. Following adoptive transfer into young mice, expression of ITGA2 was fully
282 restored to levels comparable to that of young Treg (**Sup. Fig. 7 C-E**), while MCAM in aged Treg was
283 partially restored (**Sup. Fig. 7 F-H**). These findings suggest that ITGA2 and MCAM are Treg-expressed
284 proteins that directly or indirectly support OPC differentiation, are decreased with age and
285 expression of which can be restored when aged Treg are adoptively transferred into a young
286 environment.
287
288 **Discussion**
289
290 Ageing is one of the strongest risk factors associated with the transition from relapsing-
291 remitting to secondary progressive MS[12], a phase that is characterised by the accumulation of
292 neurodegeneration and irreversible disability. This is partly due to impaired remyelination with age,
293 which was first described in animal models of remyelination[9,10] but has now also been observed in
294 MS patients[8,11]. Several factors have been linked to age-associated myelin regeneration failure, such
295 as impaired myelin debris phagocytosis by microglia and macrophages[19,20,47], reduced intrinsic
296 capacity of OPCs to differentiate into myelin-forming oligodendrocytes[13,17] and a refractory CNS
297 environment with increased stiffness and changes in extracellular matrix[16,17]. Therapies that enhance

298 remyelination and prevent age-related neurological decline are an urgent unmet need. Beyond their
299 classic immune-modulatory and anti-inflammatory role, Treg have recently emerged as key
300 regulators of tissue homeostasis and regeneration in several tissues[27], including the CNS, where we
301 have previously identified Treg as key promoters of remyelination[27]. However, how ageing affects
302 the capacity of Treg to enhance myelin regeneration had not been addressed.

303 Peripheral Treg[30,42,48], as well as Treg and tissue-resident Treg increase with age, a somewhat
304 paradoxical finding given the tissue-regenerative functions of Treg and the impairment of tissue
305 regeneration with age. Here, we further expanded the murine Treg population *in vivo* and showed
306 that despite this increased cell number, aged-associated remyelination failure was not rescued.
307 These data suggest that with ageing, Treg have an intrinsically impaired myelin-regenerative
308 capacity. Ageing is known to enhance Treg senescence, limit Treg proliferation[30,42] and there are
309 conflicting reports on the effect of ageing on Treg immunosuppressive capacity[30,42]. Previous work
310 on muscle regeneration showed that aged Treg have an impaired migratory capacity that hinders
311 muscle regeneration[36]. Additionally, in a model of influenza infection, aged Treg demonstrated an
312 impaired capacity to support lung repair, which was associated with a cell autonomous impairment
313 in their regenerative programme[43]. Here, we sought to determine whether aged Treg have an
314 intrinsically impaired capacity to drive CNS myelin regeneration combining *in vitro, ex vivo* and *in*
315 *vivo* approaches.

316 Purified aged Treg failed to significantly drive OPC differentiation into MBP-expressing
317 oligodendrocytes or the myelination of organotypic cerebellar slices, which was in striking contrast
318 to young Treg, which robustly drove both biological processes. These data suggest that ageing is
319 associated with a cell-intrinsic impairment of the regenerative capacity of Treg in CNS myelin
320 regeneration. Given that IL-2-mediated Treg expansion *in vivo* is in clinical trial for MS (clinical trial
321 number NCT02424396)[49], our findings are of translational importance as they suggest that Treg
322 expansion as a potential pro-remyelination therapy may be limited in older populations.

323 We next investigated whether the regenerative capacity of aged Treg could be restored, and
324 therefore therapeutically targetable. Surprisingly, aged Treg rescued OPC differentiation and myelin
325 wrapping similarly to that of young Treg in an *in vivo* model of young spinal cord remyelination. In
326 contrast to findings in the lung[43], the CNS remyelinating capacity of Treg can be partially restored by
327 a young environment. Interestingly, in lesions of aged mice lacking Treg, young Treg partially
328 restored $Olig2^{+}CC1^{+}$ oligodendrocyte density, while aged Treg did not, suggesting that indeed young
329 Treg have a more potent regenerative capacity than aged Treg. However, neither young nor aged
330 Treg restored $Olig2^{+}$ density or remyelination caused by depletion of endogenous Treg, suggesting
331 that with age, the failure of Treg to drive remyelination is a combination of both an intrinsically
332 impaired regenerative capacity of Treg and an aged CNS that is refractory to Treg-derived pro-
333 differentiation signals. Previous studies identified a tissue repair transcriptomic signature in the skin,
334 adipose tissue, and the lung[44]. Unexpectedly, very few of these hallmark Treg tissue repair genes
335 were downregulated in aged Treg in our transcriptomic profiling studies. These data indicate that
336 although some Treg regenerative mechanisms may be common across tissues, other mechanisms
337 may be tissue-specific or process- specific[50].

338 We recognised that the impairment of myelin regenerative Treg functions with age
339 presented a new avenue to discover novel mechanisms of how Tregs support CNS remyelination and
340 the potential to identify new targets that may be of therapeutic relevance to boost remyelination.
341 Indeed, using a combined approach of Treg/OPC transcriptomic dataset cross-referencing with *in*
342 *vitro* antibody blocking assays, we identified MCAM and ITGA2 as novel candidate mediators of Treg-
343 driven OPC differentiation. These two candidates were downregulated in aged compared to young
344 Treg, likely interact directly with OPCs and inhibit young Treg-driven OPC differentiation when
345 blocked *in vitro*. Transfer of aged Treg into young mice boosted expression of ITGA2 and to a lesser
346 extent of MCAM by Treg in preliminary studies, suggesting that these are modifiable factors that can
347 be restored in aged Treg. Furthermore, recombinant ITGA2, but not MCAM, promoted OPC

348 differentiation *in vitro* suggesting that these proteins have direct and indirect roles in Treg-driven
349 OPC differentiation.

350 To our knowledge this is the first report identifying ITGA2 as a novel mediator of Treg-driven
351 OPC differentiation, that is decreased with age, and can directly promote OPC differentiation. This
352 aligns with previous reports showing that other integrins are involved in oligodendrocyte
353 development[51] and shows that Treg are additional cellular contributors to integrin-mediated OPC
354 differentiation. MCAM has previously been described as a cell-adhesion molecule contributing to
355 brain inflammation by facilitating pathogenic T cell extravasation into the CNS[52–54] and here, we
356 identify a putative regenerative function of MCAM expressed by Treg. Together these data
357 contribute to the growing evidence that Treg express MCAM[55,56] and suggests a potential
358 regenerative role mediating Treg-stem cell interactions. Even though our data show that, *in vitro*,
359 non-activated natural Treg require direct OPC-Treg contact to drive OPC differentiation, previous
360 work from our laboratory showed that activated Treg secretome also enhanced OPC
361 differentiation[27]. Thus, Treg-mediated regenerative capacity likely involves a range of signalling
362 molecules that regulate OPC-Treg interaction as well as subsequent OPC differentiation and
363 remyelination, providing a range of potential novel mechanisms to explore as therapeutic targets for
364 remyelination therapy in the future.

365 Collectively, these studies have identified that ageing is associated with a cell-intrinsic
366 impairment of the myelin-regenerative functions of Treg. This discovery increases the range of
367 remyelination-associated mechanisms that are impaired with age[9,10,13,17–20,47]. Encouragingly, we
368 have shown that this impairment can be rescued in a young environment *in vivo*. We have also
369 identified two novel mediators of Treg-driven OPC differentiation, MCAM and ITGA2. This study has
370 identified novel mechanisms involved in CNS regeneration which need to be further investigated to
371 determine if they hold therapeutic potential for patients with demyelinating diseases.

372

373 **Methods**

374

375 **Animals**

376 All mice were on a C57BL/6J background and were either bred in-house or purchased from Charles
377 River Laboratories, UK. *Foxp3*$^{tm3(DTR/GFP)Ayr}$/J (Foxp3-DTR) mice were a kindly provided by Prof.
378 Alexander Rudensky (Memorial Sloan Kettering Institute, New York) and C57BL/6-*Foxp3*^{tm1Flv}/J
379 Foxp3-IRES-mRFP (Foxp3-RFP) mice were a kind gift from Dr. Rebecca Ingram. Neonatal C57BL6/J P3-
380 P7 pups were used for OPC and brain slice preparations, which were combined with natural Treg
381 were isolated exclusively from young (3-4m) and aged (15-18m) C57BL6/J male mice for use with
382 neonatal mixed sex pups. For *in vivo* Treg adoptive transfer studies, natural Treg were isolated from
383 young (3-4m) and aged (15m) C57BL6/J female mice or Foxp3-RFP mice, and were injected into both,
384 female and male recipient Foxp3-DTR mice (2-4m). To deplete Foxp3^{+} cells in Foxp3-DTR mice,
385 diphtheria toxin was administered as described below. All animal maintenance and experiments
386 were done in accordance with the UK Home Office regulation (Project Licences 2789 and 2894) and
387 were approved by the Queen's University Belfast's Animal Welfare and Ethical Review Committee.

388

389 **Flow cytometric analysis of healthy murine CNS**

390 Male C57BL/6 mice (8-week-old and 75 and 95-week-old) were injected i.v. with biotinylated CD45
391 antibody (30-F11, eBioscience) 3 minutes prior to euthanasia via a schedule 1 method. Brain, spinal
392 cord and spleen tissues were dissected out and placed individually into 5mL cold FACS buffer (2%
393 FCS in PBS). Single cell suspensions were prepared from brain and spinal cord tissues as previously
394 described[57]. Briefly, tissues were chopped into small pieces and digested for 30 min at 37°C with 0.4
395 mg/mL collagenase D (Sigma-Aldrich), 300 µg/mL hyaluronidase (Sigma-Aldrich) and 40 µg/mL
396 DNase 1 (Sigma-Aldrich) in IMDM supplemented with 2 mM MgCl2, 2 mM CaCl2, 2 mM l-Glutamine
397 (Sigma-Aldrich), 1 mM Sodium Pyruvate (Gibco) 10 mM HEPES (Gibco), 20% FBS and 1X Gentamycin
398 (Abcam), followed by filtration (through 100 µm mesh) and enrichment for leukocytes by gradient
399 centrifugation (40% Percoll GE healthcare, 600 x g, 15 min). To prepare single cell suspensions from

400 spleen tissues, the spleen was mechanically disrupted between two glass slides, filtered through 100
401 µm mesh and red blood cells were lysed. Splenocytes were counted using a Countess automated cell
402 counter. Following cell preparation, non-specific binding was blocked using 2.4G2 supernatant.
403 Initial staining included eBioscience Fixable Viability Dye e780 (1:4000, eBioscience) and a
404 fluorescence-tagged streptavidin to identify leukocytes which were from contaminating blood using
405 the injected CD45-biotin (1:1000, eBioscience, Clone 30-F11). Next, a 1h surface stain was performed
406 including antibodies for CD45 (1:500; eBioscience, Clone 30-F11), CD4 (1:500; eBioscience, Clone
407 GK1.5), CD8 (1:1000 Biolegend, Clone 53-6.7), CD62L (1:1000; eBioscience, Clone Mel-14), CD11b
408 (1:500; eBioscience, Clone M1/70), CD44 (1:500; Biolegend, Clone IM7), CD69 (1:100, eBioscience,
409 Clone H1.2F3), CD25 (1:200; eBioscience, Clone PC61) and CD19 (1:250, eBioscience, Clone ID3)
410 Subsequently, cells were fixed and permeabilised with the eBioscience Foxp3 staining kit
411 (eBioscience) and a 1h intracellular stain for Foxp3 was added (1:100, eBioscience, Clone FJK-16s;
412 Miltenyi, Clone REA788). For brain and spinal cord, the entire sample was acquired. Flow cytometry
413 data were acquired on a Cytek Aurora and data collection performed using SpectroFlo (Cytek).
414
415 **Lysolecithin-induced spinal cord demyelination *in vivo***
416 Spinal cord demyelination was induced as described previously[27]. In brief, demyelination was
417 induced in the ventral white matter funiculus of the thoracic spinal cord (between vertebrae T11-12
418 or T12-13) by the injection of 1.2 µL of 1% (w/v) L-α-Lysophosphatidylcholine (Lysolecithin; Sigma-
419 Aldrich) under general anaesthesia. At 7-, 10- or 14-days post lesion (dpl), mice were terminally
420 anaesthetised with intraperitoneal (i.p.) pentobarbital injections and transcardially perfused with
421 ice-cold phosphate buffered saline (PBS) followed by 4% paraformaldehyde (PFA) (Sigma-Aldrich).
422 Spinal cords were dissected and immersed overnight in 4% PFA at 4 °C. Next, spinal cords were
423 cryoprotected with 30% sucrose (Sigma-Aldrich) in PBS for 72h and snap-frozen in OCT (Tissue-Tek).
424 Frozen spinal cords were cryosectioned at 12 µm thickness and immunostained as described below.
425

426 **EAE induction**

427 Young (3-4m) and aged (15m) old C57BL/6J female mice were acquired from Charles River
428 Laboratories. Anesthetised mice were immunised with subcutaneous injections of 150 µg of MOG_{35-}
429 $_{55}$ (GenScript) emulsified in 200 µl of complete Freud's adjuvant (CFA) (Incomplete Freund's Adjuvant
430 containing 2.5 mg/mL Mycobacterium tuberculosis H37Ra, both BD Biosciences). At 0- and 2-days
431 post-immunisation, mice were injected with 200 ng of pertussis toxin intraperitoneally (PHZ1174,
432 Thermofisher). EAE clinical signs and weight were monitored daily from 7 days post-immunisation.
433 Mice were euthanised at 36 days post-immunisation by transcardial perfusion with PBS followed by
434 4% PFA. Spinal cords were dissected and immersed overnight in 4% PFA at 4 °C. Next, spinal cords
435 were cryoprotected with 30% sucrose (Sigma-Aldrich) in PBS for 72h and snap-frozen in OCT (Tissue-
436 Tek). Frozen spinal cords were cryosectioned at 12 µm thickness and immunostained as described
437 below.

438

439 ***In vivo* Treg expansion**

440 Young (2-3m) and aged mice (15m) were intraperitoneally injected with IL-2/anti-IL-2 antibody
441 complexes to expand endogenous Treg[58]. In brief, murine IL-2 (1 µg; Peprotech) was mixed with anti-
442 mouse IL-2 (5 µg; Bioxcell, Clone JES6-1A12) in PBS at 37 °C for 30 min. Each mouse was injected
443 daily for 3 consecutive days with IL-2 (1 µg) and anti-IL-2 (5 µg) in 200µl of PBS. Adequate Treg
444 expansion was assessed by flow cytometry as described below. Spinal cord demyelination was
445 induced on the day after the third injection of IL-2/anti-IL-2, by injecting lysolecithin into the
446 ventrolateral white matter as described above. Treg expansion was examined by flow cytometry as
447 described below on day 10dpl in aged mice, while OPC differentiation was examined at 7 dpl in
448 young mice and 10 dpl in aged mice.

449

450 ***In vivo* Treg depletion and adoptive transfer of wild type natural Treg**

451 Young (2-4m) and aged (19-23m) male and female Foxp3-DTR mice were injected daily i.p. with
452 diphtheria toxin (DT; 0.04 µg/g of body weight; Sigma, Cat. No. D0564) for 3 days prior to
453 demyelination. To maintain endogenous Treg depletion during remyelination, DT (0.04 µg/g of body
454 weight) was injected i.p. every fourth day. Control animals received 200 µl of saline i.p. Depletion
455 was confirmed at the endpoint by flow cytometric analysis of endogenous GFP^+ natural Treg in
456 blood, spleen, and lymph nodes (see below). To adoptively transfer young (2-4m) and aged (15m)
457 natural Treg to Treg-depleted mice, we immunomagnetically isolated natural Treg from wild type
458 female mice or Foxp3-RFP male and female mice using a $CD4^+$ and $CD25^+$ Treg isolation kit
459 (STEMCELL Technologies) as described below. For remyelination experiments, mice were injected
460 i.p. with 10^6 wild type natural Treg (which are resistant to DT) in the 24h prior to lysolecithin-induced
461 demyelination, while in the case of adoptive transfer of RFP^+ Treg to evaluate MCAM and ITGA2
462 expression, 4 x 10^5 cells per mouse were injected to non-lesioned mice. Reconstitution was
463 evaluated by flow cytometry in lymph nodes at the endpoint (see below).
464
465 **OPC isolation and culture**
466 OPCs were isolated from P3-P7 mice based on A2B5 expression. Briefly, pups were culled by an
467 overdose of pentobarbital (200 mg/mL, 20µl per mouse) and whole brain was dissected and placed
468 in ice-cold Hibernate-A (ThermoFisher Scientific). Dissected brain was minced using scalpels,
469 transferred to a 15mL tube, and centrifuged for 1 min at 100 g and 4 °C. Hibernate-A medium was
470 aspirated, and the pellet was resuspended in 5 mL dissociation media containing 165U of Papain
471 (Worthington) and DNAse type I (40 µg/mL; Worthington) in hibernate A for 30 min at 37 °C. Upon
472 digestion papain was washed off with Hanks Buffered Salt Solution (HBSS) (ThermoFisher Scientific)
473 and cells were centrifuged for 5 min at 300 g and 4 °C. The pellet was resuspended in 4 mL
474 trituration buffer (Hibernate-A with 2% B27; ThermoFisher Scientific) and 2 mM sodium pyruvate
475 (ThermoFisher Scientific) and gently triturated ten times using a 5 mL pipette. Tissue was left to
476 settle for 2 min at room temperature (RT), and supernatant was transferred to a clean 50 mL tube

477 through a 70 µm strainer (Corning). Remaining tissue was exposed to another 2 mL of trituration
478 buffer and gently triturated using a glass polished pipette. After trituration, tissue was left to settle
479 for 2 min at RT and supernatant was transferred to the tube through the 70 µm strainer. This step
480 was repeated another time with a glass fire-polished pipette of decreased diameter and then with a
481 1 mL pipette. To further remove debris from the cell suspension, 11.5 mL of 90% Percoll (GE
482 Healthcare) diluted in 10X PBS (ThermoFisher Scientific) was added and topped up to a final volume
483 of 45 mL with Dulbecco's Modified Eagle's medium (DMEM) (ThermoFisher Scientific). The cell
484 suspension was then centrifuged at 800 g for 20 min at 4 °C. Upon centrifugation, the pellet was
485 washed with HBSS and then resuspended in 10 mL magnetic-activated cell sorting (MACS) buffer
486 (Hibernate-A with 2 mM sodium pyruvate, 2% B27, 0.5% BSA; ThermoFisher Scientific), 2 mM EDTA
487 (Sigma-Aldrich) and 10 µg/mL insulin (Sigma-Aldrich), and incubated for 30 min at 37 °C in a 10 cm
488 petri dish coated with BSC1 Griffonia Simplicifolia Lectin (BSL1, 5 µg/mL)(Vektor Labs) to remove
489 microglia. Then, the supernatant was collected, and cells were counted and centrifuged at 300 g for
490 5 min at 4 °C. The pellet was resuspended and incubated with 2 µg of A2B5 antibody (Millipore,
491 Clone A2B5-105) in 500 µL of MACS buffer per 10 million cells for 25 min on ice, with gentle
492 resuspensions every 10 min. Cells were washed with HBSS and spun at 300 g for 5min at 4 °C
493 (Miltenyi Biotec). The pellet was resuspended and incubated with 80 µL of MACS buffer and 20 µL of
494 anti-IgM microbeads (Miltenyi Biotec) for 15 min. Then, cell suspensions were centrifuged at 300 g
495 for 5 min at 4 °C, resuspended in 0.5 ml MACS buffer and placed in a MACS mini column (Miltenyi
496 Biotec) on a MiniMACS Separator (Miltenyi Biotec) and washed with 1.5mL MACS buffer. Once the
497 liquid passed completely through the column, the column was removed from the stand and placed
498 in a new 15 mL tube, where 1 mL of OPC media was added to the column and plunged through to
499 elute the OPCs. OPC media contained DMEM, 2% B27, sodium pyruvate (2 mM), insulin (5 µg/mL),
500 Trace Elements B (0.01%; Corning), Forskolin (5 µM; Sigma-Aldrich), Biotin (10 ng/mL; Sigma-
501 Aldrich), Penicillin-streptomycin-glutamine (1%; ThermoFisher Scientific), N-acetyl cysteine (60
502 µg/mL; Sigma-Aldrich) and 1% SATO stock solution. SATO stock solution contained bovine serum

503 albumin (BSA) fraction V (0.1 mg/mL; ThermoFisher Scientific), sodium selenite (4 µg/mL; Sigma-
504 Aldrich), putrescine (1.61 mg/mL; Sigma-Aldrich), apo-transferrin (0.1 mg/mL; Sigma-Aldrich) and
505 progesterone (4 µg/mL; Sigma-Aldrich). The purified population was counted and diluted in OPC
506 media for plating. OPCs were plated at a density of 3,000 cells per well in 96-well plates (Falcon)
507 previously coated with poly-L-lysine (10 µg/mL; Sigma-Aldrich) and laminin (10 µg/mL; Sigma-
508 Aldrich) diluted in DMEM. OPCs were plated with PDGFaa (20 ng/mL; Peprotech) and NT-3 (10
509 ng/mL; Peprotech). The following day two thirds of the media was removed (100 µl) and 100 µl of
510 fresh OPC media with PDGFaa (20 ng/mL) and NT3 (10 ng/mL) were added per well. Cells were
511 incubated at 37°C and 5% CO_2 for two days. On the third day, media was completely removed and
512 20,000 Treg in fresh media were added as indicated below.
513 For transwell assays, OPCs were selected with anti-PDGFRα panning. After microglia depletion in
514 BSL1-coated petri dishes, the supernatant was transferred to PDGFRα panning plates and incubated
515 at RT for 1 h. PDGFRα panning plates were coated with goat-anti-rat IgG (H+L) (7.5 µg/mL;
516 ThermoFisher Scientific) in PBS with 0.2% BSA and rat anti-PDGFRα (1.5 µg/mL in PBS; BD
517 Biosciences) with 0.2% BSA for 3 h. Supernatants were removed, cells were washed 5-8 times with
518 PBS and the attached OPCs were scraped, counted, and replated in 24-well plates (Sarstedt) at
519 10,000 cells per well. On the third day *in vitro* 50,000 Treg were added either directly into the well
520 with OPCs or in a transwell (Millipore) above the OPCs.
521 For recombinant ITGA2 and MCAM treatment, OPC were treated with increasing concentrations of
522 the recombinant proteins in OPC media, or vehicle control, on the day of growth factor removal.
523 Cells were cultured for 3 days in the case of ITGA2 and 6 days in the case of MCAM without any
524 further media changes.
525 At the endpoint (3 or 6 days after treatment) OPC were fixed for 15 min with 4% PFA and washed
526 twice with PBS prior to immunostaining. Cells were blocked with 5% donkey serum (Sigma-Aldrich)
527 with 0.1% Triton-X-100 (Sigma-Aldrich) in PBS for 1h at RT. OPCs were then stained overnight at 4 °C
528 with primary antibodies diluted in blocking solution against Olig2 (1:500, Bio-techne), CNPase (1:500,

529 Sigma-Aldrich, clone 11-5B), MBP (1:500, Millipore, clone 12), Ki67 (1:300, Abcam, clone SP6), NG2
530 (1:200, Millipore), and CD3 (1:500, eBioscience). Cells were then washed three times with PBS and
531 incubated for 1 h at room temperature with secondary antibodies diluted in blocking buffer (Alexa
532 fluor (AF) 488 donkey anti- rabbit (1:500; ThermoFisher Scientific), AF568 donkey-anti- rat (1:500;
533 Abcam), AF647 donkey anti-mouse (1:500; Abcam), AF647 donkey anti-rabbit (1:500; ThermoFisher
534 Scientific) and AF755 donkey anti-goat (1:500; ThermoFisher Scientific) and Höechst (1:10,000;
535 Sigma-Aldrich). Cells were then washed with PBS three times and stored in 150 µL PBS/well for cell
536 imaging.
537 Cell imaging was performed using the CellInsight CX5 high content imaging system (ThermoFisher
538 Scientific) for 96-plates and EVOS for 24-well plates. Twenty-five separate fields of view of each well
539 in 96-well plates and the cell populations of interest were quantified using CellInsight CX5 analysis
540 software and the SpotCounts programme. For 24-well plates we imaged randomly 5 fields of view
541 per well at 20X magnification and images were analysed manually with Fiji.
542
543 **Natural Treg isolation**
544 Young (2-4 m) and aged (15-18 m) male mice were culled by CO_2 overdose. Spleens and lymph nodes
545 were removed and mashed through a 70 µm strainer with a 2 ml syringe plunger. $CD4^+$ T cells were
546 immunomagnetically purified by negative selection according to manufacturer's instructions
547 (STEMCELL Technologies). Isolated $CD4^+$ T cells were then subjected to a $CD25^+$ cell isolation
548 (STEMCELl Technologies) using releasable magnetic spheres (STEMCELL Technologies) according to
549 the manufacturer's protocol. Purity was confirmed by flow cytometry for CD4, CD25 and Foxp3 (**Sup.
550 Fig. 2A**). For i.p. injections in adoptive transfer experiments, cells were resuspended at 10^6 cells per
551 200 µL in saline. For OPC-natural Treg co-cultures 20,000 natural Treg were resuspended in 150 µl of
552 OPC Brainphys-based media and added to OPCs in 96-well plates. For 24-well transwell plate
553 experiments 50,000 natural Treg were resuspended in 250 µl OPC-BrainPhys media and added to
554 transwells above cultured OPCs. OPC BrainPhys-based media contains BrainPhys (STEMCELL

555 Technologies), B27 (2%; ThermoFisher Scientific), Glutamax (0.5 mM; ThermoFisher Scientific), N-
556 acetyl-cysteine (60 µg/mL), SATO (1:100, as described above) and insulin (5 µg/mL). In the case of
557 brain slices, 50,000 Treg were diluted in 5 µL of brain slice media and dropped directly onto brain
558 slices.
559 For natural Treg mechanistic studies, OPCs and Treg were isolated as described above. Prior to OPC-
560 natural Treg co-culture, 120,000 Treg were transferred to a 1.5 mL microcentrifuge tube and
561 centrifuged at 400 g for 5 min at 4 °C. Treg were resuspended in 100 µL of PBS with 2% FCS and a
562 blocking antibody (20 µg/mL) or corresponding isotype were added per tube. Natural Treg were
563 incubated with the blocking antibody for 45 min on ice and then cells were washed with PBS and
564 centrifuged for 10 min at 400 g and 4 °C. Cells were resuspended in 900 µl of OPC BrainPhys-based
565 media (see above) and 20,000 Treg in 150 µL of media were added per well in 96-well plates. As
566 previously, Treg were co-cultured with OPCs for 7 days *in* vitro (DIV) and then fixed and stained as
567 described above. Blocking antibodies used were anti-NK1.1 PE (eBioscience, clone PK136), anti-
568 CD62L-APC (eBioscience, clone Mel14), anti-Ly6c1-APC (eBioscience, clone RB6-BC5), rat-isotype-
569 APC (eBioscience), anti-Itga2 (Abcam, clone EPR5788), anti-MCAM (Abcam, clone EPR3208) and
570 rabbit-isotype (Vektor labs).
571
572 **Organotypic brain slice cultures**
573 Brainstem slices from male and female P3 C57BL/6J mice were prepared at 300 µm thickness using a
574 McIlwain Tissue Chopper as described previously[27]. Slices were separated and placed on Millicell
575 inserts in individual wells of a 24-well plate (Millipore) with 250 µl brain slice medium containing
576 46.6% minimum essential medium (ThermoFisher Scientific), 25% Earls balanced salt solution
577 (Sigma-Aldrich), 25% heat-inactivated horse serum (Thermofisher Scientific), 1% penicillin-
578 streptomycin (Thermofisher Scientific), 1% glutamax (Thermofisher Scientific) and 1.4% D-glucose
579 (Sigma). Brain slices were incubated at 37 °C and 5% CO_2 overnight and then media was fully
580 replaced. On day 3, media was changed again and 50000 young or aged Treg were added directly on

581 top of each slice in a 5 µl droplet. Brain slices were cultured for a further 7 DIV, with media changes
582 every other day. On day 10 (7 days post-treatment), brain slices were fixed with 4% PFA for 45 min
583 and immunostained. In brief, brain slices were blocked for 2 h in 10% normal donkey serum (Sigma-
584 Aldrich), 1 mM Hepes (Thermofisher Scientific), 1% BSA (ThermoFisher Scientific) and 0.5% Triton X-
585 100 (Sigma-Aldrich) in PBS. Slices were incubated with primary antibodies for rat anti-MBP (1:500;
586 Millipore, clone 12) and chicken anti-NFH (1:500; EncorBiotech, polyclonal) in blocking buffer at 4 °C
587 for two overnights. Brain slices were then washed with PBS-0.01% triton three times for 30 min.
588 Slices were incubated with secondary antibodies (AF488 donkey anti-chicken IgY (1:500; Abcam,
589 polyclonal) and AF568 donkey anti-rat IgG (1:500; Abcam, polyclonal) in blocking buffer overnight at
590 4 °C. Brain slices were washed twice with PBS-0.01% triton and then incubated with Höechst stain
591 (1:20000; Sigma-Aldrich) for 10 min. Slices were washed with PBS and mounted using fluoromount G
592 (Thermofisher Scientific). Imaging was performed using a Leica SP8 confocal microscope, using a 63X
593 oil objective and the Leica Navigator at 0.5 µm intervals over 10 µm. Four fields of view per brain
594 slice were selected for imaging based on NFH and Höechst staining but blinded to MBP. To quantify
595 myelination index, the area stained by NFH, MBP and the colocalising area of NFH^+MBP^+ were
596 measured per stack in Fiji[59] using a Fiji plug-in developed and kindly provided by the Williams
597 laboratory at the University of Edinburgh[60]. Then, the ratio between total NFH^+ and NFH^+MBP^+ areas
598 (myelination index) was calculated per z-stack and the average of the myelination index per slice was
599 calculated.
600
601 **Flow cytometry**
602 Spleens and lymph nodes were mashed through a 70 µm strainer. For splenocytes, cells were
603 exposed to red blood cell lysis buffer (STEMCELL Technologies) for 2 min at room temperature. Both,
604 lymph nodes and splenocytes were then washed with PBS and centrifuged at 300 g for 5 min at 4°C.
605 Cells were resuspended in 200 µL PBS and stained with a cell viability dye with eFluor 506-UV
606 viability dye (1:2000; ThermoFisher Scientific) and cell surface stained with antibodies for CD4

607 (1:500; eBioscience, clone RM4.5), CD25 (1:500; eBioscience, clone PC61.5), ITGA2 (1:50;
608 eBioscience, Clone DX5) and MCAM (1:100; Biolegend, Clone ME9F1) for 15 min at RT. Cells were
609 washed with flow cytometry staining buffer (FCSB) (2% FCS in PBS) and centrifuged at 300 g for 5
610 min at 4 °C. Cells were then fixed with Fix & Perm A (ThermoFisher Scientific) for 10 min at RT.
611 Fixative was washed off with FCSB and centrifuged at 300 g for 5 min at 4 °C. The pellet was
612 resuspended in PBS and data were acquired on a FACSCanto II or on a FACS Symphony in the case of
613 RFP+ adoptive transfer. In the natural Treg depletion experiment, presence of endogenous natural
614 Treg was determined by the expression of GFP. To determine the purity of natural Treg isolations or
615 the extent of natural Treg reconstitution by adoptive transfer, cells were washed and centrifuged for
616 5 min at 300 g and 4 °C. Cells were then resuspended in 100 µL Fix & Perm B (ThermoFisher
617 Scientific) with an anti-Foxp3 antibody (1:100; eBioscience, clone FJK-16S) overnight at 4 °C. Cells
618 were then washed with FCSB and centrifuged at 300 g and 4 °C for 5 min. Cells were then
619 resuspended, data were acquired on a FACSCanto II and analysed using FlowJo software version 9.0
620 and 10.0 (BD). To calculate cell numbers, singlets were identified by FSC-H versus FSC-A and viable
621 cells gated for CD3 and CD4, and subsequently CD25 and $Foxp3^{+}GFP^{+}$ and $Foxp3^{+}GFP^{-}$ cells. To
622 evaluate young and aged Treg numbers in blood, 30 µL were incubated with 100 µL of the viability
623 and cell surface antibody mix for 30 min at room temperature. Cells were then washed with FCSB
624 and centrifuged at 300 g for 5 min at 4 °C. After resuspension, cells were fixed and lysed in 100 µL of
625 OptiLyse B (Beckman Coulter) for 10 min at RT, washed with distilled water and then after 15 min,
626 acquired on a FACSCanto II. After initial data acquisition, cells were centrifuged at 300 g for 5 min at
627 4 °C and incubated overnight with anti-Foxp3 antibody in Fix & Perm B, as described above. Cells
628 were washed and data were acquired on a FACSCanto II. To evaluate changes in MCAM and ITGA2
629 expression upon reconstitution, splenocytes were stained as described above but without Fix &
630 Perm A or B, to avoid quenching endogenous RFP and GFP signal and data were acquired from live
631 cells on a BD FACS Symphony. To calculate cell proportions and mean fluorescence intensity, singlets
632 were identified by FSC-H versus FSC-A and viable cells gated for CD4, and subsequently RFP^{+} GFP^{-}

633 Treg. ITGA2 and MCAM expression based on median fluorescent intensity was then evaluated in
634 RFP^+ and ITGA or $MCAM^+$ RFP^+ Treg respectively.
635
636 **Immunofluorescence staining of CNS tissue**
637 Spinal cord sections were dried for 30 min at RT and washed for 10 min in PBS. For Olig2, Ki67, CC1
638 and ASPA staining, spinal cord sections underwent antigen retrieval at 85 °C for 10 min with 1X
639 citrate buffer pH 6.0 (Sigma-Aldrich). Tissue sections were washed with PBS and permeabilised with
640 1% Triton-X-100 in PBS for 30 min at RT. Sections were washed with PBS and incubated with blocking
641 solution (5% donkey serum; Sigma-Aldrich) diluted in TBS with 0.25% tween (Sigma-Aldrich) for 1h at
642 RT. If spinal cord sections were incubated with a primary antibody raised in mouse (e.g. anti-CC1)
643 sections underwent an additional 1 h blocking step at RT using Mouse on Mouse (M.O.M) blocking
644 reagent (Vector labs) in 5% donkey serum. Then spinal cord sections were incubated with primary
645 antibodies against Olig2 (1:500; Bio-Techne, polyclonal), anti-APC (1:400, Abcam, clone CC1), anti-
646 ASPA (1:300, Millipore, polyclonal), anti-NFH (1:500; Abcam, polyclonal), anti-MBP (1:500; Millipore,
647 clone 12) or anti-Ki67 (1:300; Abcam, clone SP6) overnight at 4 °C. Sections were washed with Tris-
648 Buffered-Saline (TBS) (ThermoFisher Scientific) with 0.25% Tween (Sigma-Aldrich). Secondary
649 antibodies including donkey anti-goat AF488, donkey anti-mouse AF568, donkey anti-rabbit AF647
650 (all 1:500; ThermoFisher Scientific), donkey anti-rat AF568 (1:500; Abcam), donkey anti-rabbit AF647
651 (1:500, Abcam) and Höechst (1:10000; Sigma-Aldrich) were added for 1 h at room temperature.
652 Spinal cord sections were then washed with TBS-0.25% Tween twice and mounted with fluoromount
653 G.
654 For detection of CD4 and Foxp3, spinal cord sections underwent antigen retrieval at 80 °C for 5 min.
655 After blocking with 10% NDS, sections were incubated with rat-anti-mouse CD4 (1:500; Biolegend,
656 Clone RM4.5) and rabbit-anti-mouse Foxp3 (1:500; Biotechne, polyclonal) for 1h at room
657 temperature, washed and incubated with secondary antibodies as described above.

658 Image acquisition was performed using the Leica TIRF and Leica DM5500 widefield fluorescent
659 microscopes. Further image processing was performed in Fiji[59] software and analysis was undertaken
660 by blinded manual counting. For NFH and MBP wrapping analysis, images were quantified using Cell
661 Profiler and Cell Profiler Analyst softwares[61,62].
662
663 **RNA sequencing and analysis**
664 Young (2-4m) and aged (16m-20m) natural Treg were isolated from spleen and lymph nodes by
665 magnetic-activated cell sorting and purity was checked by flow cytometry as described above (**Sup.**
666 **Fig. 3A**). Natural Treg were lysed in 0.5 mL of Trizol (Sigma-Aldrich) by vortexing and pipetting and
667 frozen at -80 °C. RNA was extracted combining Trizol and Chloform isolations with RNAeasy micro kit
668 columns (Qiagen). RNA concentration was determined using a Nanodrop, and RNA quality was
669 assessed by Qubit measurement and in an RNA nanochip Bioanalyzer. Sequencing libraries were
670 prepared using the Kapa Hyper Preparation kit with riboerase (Roche) following manufacturer's
671 instructions. Sequencing was performed on the NovaSeq 6000 in a pair-end 75 base pair format and
672 80 million reads.
673 The raw sequencing data was checked for lower quality bases and adaptor sequences with FastQC
674 and quality trimming was performed using CutAdapt[63]. The high-quality trimmed data were mapped
675 on mm10 mouse reference genome using STAR aligner (v 2.7.0a)[64]. The quantification of each gene
676 transcripts was performed with ensemble transcript annotation gtf file (GRCm38) using
677 featureCounts tool (v 2.0.0)[65]. The resultant read counts matrix was analyse using DESeq2 (v1.38.1)[66]
678 to identify differentially expressed genes between the young and aged natural Treg samples using
679 Wald tests with the Bonferroni correction for multiple testing. The differentially expressed genes
680 (DEG) with a multiple testing adjusted $p<0.05$ and fold change >2 were considered for further
681 downstream analysis. These genes were subjected to gene ontology enrichment analysis using
682 enrichGO function in clusterProfiler (v4.2) R package and DAVID (https://david.ncifcrf.gov). Over and
683 underrepresented ontology terms were identified (p value <= 0.05 and Bonferroni correction p

684 adjustment method). Next, enriched activated and suppressed functional pathways were identified
685 using gseKEGG function in clusterProfiler with p value<0.05.

686 Raw data files from RNAseq are available at the GEO database (accession number GSE218804).

687

688 **Bioinformatic analysis to identify putative Treg mechanisms**

689 To determine the molecular mechanisms associated with Treg-driven OPC differentiation that are
690 impaired with ageing, we combined our young and aged natural Treg RNA sequencing with data
691 obtained from Zhang *et al.* 2014 (GSE: 52564)[45]. We first extracted genes that were downregulated
692 in aged natural Treg and associated with the GO cellular component term "plasma membrane". We
693 then extracted the FPKM matrix and selected genes that were upregulated in OPC when compared
694 with newly myelinating oligodendrocytes and oligodendrocytes in the Zhang *et al.* database. We
695 performed GO cellular component analysis on those OPC-enriched genes and selected genes
696 associated with the GO term Apical Plasma Membrane. Then, both gene lists were subjected to a
697 protein-protein interaction analysis using the String open-source tool (www.string-db.org)[46]. Protein-
698 protein interactions within genes that were associated only with the natural Treg or only the OPC
699 databases were eliminated, and the remaining downregulated natural Treg membrane proteins
700 were prioritised considering their significance, fold change and the number of potential interactors
701 enriched in OPCs. Candidate genes were then selected based on their p-adjusted value, fold
702 enrichment and the number of interactions with OPC receptors.

703

704 **Statistical analysis**

705 All statistical analyses were performed in GraphPad Prism (GraphPad Software, Inc. version 9) or R.
706 First normality of datasets was assessed using Shapiro-Wilk and Kolmogorov-Smirnov tests. For
707 comparisons between 2 groups, such as young and aged Treg and OPC differentiation (Sup. Fig. 1),
708 unpaired two-tailed Student's t tests were used if data were normally distributed, and Mann-
709 Whitney U tests for non-parametric datasets. When more than two groups were analysed and

710 datasets were normally distributed, a one-way analysis of variance (ANOVA) was performed
711 assuming equal variances, followed by Sidak's multiple comparison test. When two factors were
712 controlling the outcome, such as replicates and treatments, 2-way ANOVA followed by Dunnet's
713 comparison was used. When datasets were was not normally distributed, a Kruskal-Wallis followed
714 by Dunn's multiple comparison test was used. For percentage data, arcsin conversion was
715 performed to analyse the data using parametric tests. For all statistical tests, differences were
716 considered significant at $p<0.05$.
717
718 **Data and code availability**
719 Young and aged natural Treg RNA sequencing data generated in this study are available at GEO
720 (accession number: GSE218804).
721
722 **Figure legends**
723
724 **Figure 1: Treg frequency is increased in the aged CNS. A** Flow cytometric plot and **B** quantification
725 showing the proportions of natural Treg (endogenous GFP reporting Foxp3 expression in Foxp3-DTR
726 mice) in aged blood compared to young circulation (n=30-32 mice, unpaired two-tailed Student's t
727 test after *arcsin* conversion). **C** Flow cytometric plot and **D** quantification of Treg proportion,
728 identified by CD4 and Foxp3 expression in young and aged mouse spleens (n=15-32 mice, unpaired
729 two-tailed Student's t test after *arcsin* conversion). **E** Quantification of tissue resident Treg
730 proportion, identified by CD69 expression (n=8-13 mice, unpaired two-tailed Student's t test after
731 *arcsin* conversion). **F-H** Violin plot-based quantification showing the proportion and count of Treg
732 and tissue resident Treg in the spinal cord of healthy young and aged mice (n=8-13 mice, unpaired
733 two-tailed Student's t test after *arcsin* conversion). **I-K** Violin plot-based quantification showing the
734 proportion and count to Treg and tissue resident Treg in the brain of healthy young and aged mice
735 (n=8-13 mice, unpaired two-tailed Student's t test after *arcsin* conversion). **L** Immunostaining of

736 DAPI (blue), CD4 (green) and Foxp3 (magenta) Tregs (highlighted with yellow arrows) in a
737 demyelinated lesion from mice with EAE (scale bar = 50 µm). **M** Quantification of the density of $CD4^+$
738 $Foxp3^+$ Treg in lysolecithin-induced demyelinated lesions at 3 and 14 dpl (n=3-7 mice, 2-way
739 ANOVA). **N** Quantification of the density of $CD4^+$ $Foxp3^+$ Treg in EAE-induced demyelinated lesions at
740 36 days post-immunisation (n=3-4 mice, unpaired two-tailed Student's t-test).
741
742 **Figure 2: Expansion of Treg does not rescue impaired OPC differentiation in aged mice. A** Flow
743 cytometric plot showing CD25 and Foxp3 expression of control aged mice and aged mice treated
744 with intraperitoneal injection of IL-2/anti-IL-2 complexes **B, C** Quantification of $CD25^+Foxp3^+$ natural
745 Treg proportion in a $CD4^+$ T cell population from the spleen and blood of control aged mice and aged
746 mice treated with intraperitoneal injection of IL-2/anti-IL-2 complexes (n=3, unpaired two-tailed
747 Student's t test after *arcsin* conversion). **D** Representative images of OLIG2 (cyan) and CC1 (magenta)
748 immunostaining in young control and Treg expanded demyelinated lesions at 7dpl (scale bar = 50
749 µm, lesion area demarcated with the dotted bar). **E, F** Quantification of $OLIG2^+$ cell density and
750 $OLIG2^+CC1^+$ cell density in the demyelinated area of young control and Treg expanded mice (n=4-5
751 mice, unpaired two-tailed Student's t-test). **G** Representative images of OLIG2 (cyan) and CC1
752 (magenta) immunostaining in aged control and Treg expanded demyelinated lesions at 10dpl (scale
753 bar = 50 µm, lesion area demarcated with the dotted bar). **H, I** Quantification of $OLIG2^+$ cell density
754 and $OLIG2^+CC1^+$ cell density in the demyelinated area of age control and Treg expanded mice (n=6-7
755 mice, unpaired two-tailed Student's t-test). **J** Representative images of NFH (cyan) and MBP
756 (magenta) immunostaining in aged control and Treg expanded demyelinated lesions at 10dpl (scale
757 bar = 50 µm, lesion area demarcated with the dotted bar). **K, L** Quantification of NFH^+ axon density
758 and NFH^+MBP^+ axon density in the demyelinated area of aged control and Treg expanded mice (n=6-
759 7 mice, unpaired two-tailed Student's t-test).
760

761 **Figure 3: Aged natural Treg demonstrate impaired capacity to drive OPC differentiation and**
762 **myelination *in vitro*. A** Representative images of OPCs co-cultured with young and aged natural Treg
763 and immunostained for OLIG2 (cyan) as a pan oligodendrocyte lineage marker, the proliferation
764 marker Ki67 (magenta). **B** Quantification of OPC proliferation when co-cultured with young and aged
765 natural Treg (n=6, 1-way ANOVA after *arcsin* conversion). **C** Representative images of OPCs co-
766 cultured with young and aged natural Treg and immunostained for OLIG2 (cyan) and differentiation
767 markers CNP (grey) and MBP (magenta) (**C**) (scale bar = 100 µm). **D** Quantification of the proportion
768 of OPCs reaching early stage-differentiation when exposed to young and aged natural Treg, as
769 indicated by CNPase staining (n=9, 1-way ANOVA after *arcsin* conversion). **E** Quantification of the
770 proportion of OPCs expressing late-stage differentiation marker MBP in control and OPCs treated
771 with young and aged natural Treg (n=9, 1-way ANOVA, Sidak's multiple comparisons test). **F**
772 Immunohistochemistry of control and young and aged Treg treated cerebellar slices (MBP, magenta
773 and NFH, green, scale bar = 100 µm). **G** Quantification of myelination index (ratio between MBP and
774 NFH colocalization area and NFH area) and myelination index fold change in neonatal cerebellar
775 slices (n=9 mice, 1 brain slice per mouse, 3 independent experiments, 1-way ANOVA after *arcsin*
776 conversion, Sidak's multiple comparison tests).
777
778 **Figure 4: Myelin-regenerative capacity of aged Treg is restored in a young environment. A** Diagram
779 explaining the experimental design of *in vivo* Treg depletion, Treg adoptive transfer and spinal cord
780 demyelination. **B**, **C** Representative images of immunostaining identifying oligodendrocytes by the
781 co-localisation of the pan-oligodendrocyte lineage marker OLIG2 (green) with CC1 (magenta, **B**) or
782 ASPA (magenta, **C**) at 14 dpl (scale bar = 100 µm, demyelination area is highlighted by the white
783 line). **D-F** Bar graphs show the quantification of total number of oligodendrocyte lineage cells, as
784 well as CC1-expressing or ASPA-expressing oligodendrocytes in the demyelinated lesions of PBS
785 control mice, natural Treg-depleted mice and mice depleted of endogenous Treg that received
786 young or aged natural Treg by adoptive transfer (n=7-9, 1-way ANOVA, Sidak's multiple comparisons

787 test). **G** Representative images of immunostaining for neurofilament-H (NFH, green) and MBP
788 (magenta) to quantify myelin wrapping as an early marker of remyelination at 14 dpl (scale bar = 100
789 µm, demyelination area is highlighted by the white line). **H-J** Quantification shows the total number
790 of axons, the density of MBP wrapped axons and the percentage of MBP-wrapped axons from the
791 total number of axons (n=6-9, 1-way ANOVA, Sidak's multiple comparisons test).
792
793 **Figure 5: Young Treg only partially rescue oligodendrocyte differentiation in aged Treg-depleted**
794 **mice. A** Representative images of immunostaining identifying oligodendrocytes by the co-
795 localisation of the pan-oligodendrocyte lineage marker OLIG2 (green) with CC1 (magenta) at 14 dpl
796 (scale bar = 100 µm, demyelination area is highlighted by the white dotted line). **B-D** Bar graphs
797 show the quantification of total number of oligodendrocyte lineage cells, as well as $Ki67^+$
798 proliferating OPCs and $CC1^+$ oligodendrocytes in the demyelinated lesions of PBS-treated control
799 aged mice, natural Treg-depleted aged mice and aged mice depleted of endogenous Treg that
800 received young or aged natural Treg by adoptive transfer (n=4-6 mice, 1-way ANOVA, Sidak's
801 multiple comparisons test).
802
803 **Figure 6: Ageing significantly alters natural Treg transcriptome. A** Principal component analysis
804 demonstrating the clustering differences between young and aged natural Treg. **B** Volcano plot
805 demonstrating 1456 genes upregulated and 302 genes downregulated genes in aged natural Treg
806 relative to young Treg. **C** Heatmap demonstrating hierarchical clustering of the top 50 differentially
807 expressed genes between young and aged Treg. **D** Graph showing the pathways enriched amongst
808 differentially expressed genes. **E** Bar graph highlighting the GO biological processes associated with
809 genes that are upregulated or downregulated in aged Treg. **F** Heatmap showing the normalised
810 count values for the Treg tissue repair programme identified by Delacher *et al.*[44] **G** Graph showing
811 the Treg tissue repair programme signature genes score in aged and young natural Treg.
812

813 **Figure 7: Natural Treg-driven OPC differentiation *in vitro* is contact-dependent. A** Representative
814 images of immunostaining showing cell-to-cell contact between OPCs and Treg in OPC-Treg co-
815 cultures *in vitro*. OPCs are identified by the co-staining of OLIG2 (cyan) and NG2 (grey), while Treg
816 are identified by CD3 (red) (scale bar = 50 µm). **B** Representative images showing Treg ($CD4^+$ (green),
817 $Foxp3^+$ (magenta)) in close proximity or direct contact with $OLIG2^+$ oligodendrocyte lineage cells in
818 demyelinated lesions in mice with EAE, highlighted by the yellow arrows (scale bar=25µm). **C**
819 Representative images of immunostaining of OPCs directly co-cultured with young Treg and OPCs
820 cultured with young Treg in a transwell (OLIG2 (cyan) and MBP (magenta), scale bar=100µm). **D**
821 Quantification of MBP-expressing oligodendrocytes in control OPCs, OPCs directly co-cultured with
822 young Treg and OPCs cultured with young Treg in a transwell (n=6, 1-way ANOVA after arcsin
823 conversion, Sidak's multiple comparison's test). **E** Diagram summarising bioinformatic approaches to
824 identify protein-protein interactions between OPCs and Treg. **F** Graph showing 21 protein candidates
825 expressed in the Treg plasma membrane, that are downregulated in aged Treg and have potential
826 bindings partners enriched in OPCs vs oligodendrocytes. Log_2 Change, $-Log_{10}$ (Padj) and the number
827 of OPC binding partners are indicated (see legend). **G** Bar graphs showing RNAseq normalised count
828 values for the top 6 candidates.
829
830 **Figure 8: *Mcam* and *Itga2* contribute to Treg-driven OPC differentiation and are downregulated in**
831 **aged Treg. A** Representative images of immunostaining showing OPC differentiation in co-culture
832 with young Treg in the presence or absence of neutralising antibodies against candidate cell surface
833 mediators (scale bar = 100 µm). **B, C** Bar graphs showing the quantification of OPC differentiation
834 measured by the fold change in percentage of MBP^+ cells and MBP^+ area per well (n=7, 2-way
835 ANOVA, Dunnett's multiple comparison tests). **D** Representative images of immunostaining showing
836 OPC differentiation in neonatal OPCs treated with recombinant ITGA2 (OLIG2 (cyan), CNPase (grey)
837 and MBP (magenta), scale bar = 50 µm). **E, F** Bar graphs showing quantification of the proportion of
838 MBP-expressing oligodendrocytes and total MBP area per well in rITGA2-treated neonatal OPCS at 3

839 days *in vitro* (n=7 mice, 2 independent experiments, 1-way ANOVA, Dunnett's multiple comparison
840 test). **G** Sholl analysis showing the number of intersections as a function of the distance from the cell
841 body to determine changes in the morphology of MBP-expressing oligodendrocytes (n=7 mice, 3
842 wells per mice and 6-9 cells per well were analysed, 2-way ANOVA).
843
844 **Supplementary information**
845
846 **Supplementary Figure 1: $CD4^+$ and $CD8^+$ T cells are increased in the aged CNS. A-D** Violin plot-based
847 quantification showing the proportion and count of $CD4^+$ and $CD8^+$ T cells in the spinal cord of
848 healthy young and aged mice. **E-H** Violin plot-based quantification showing the proportion and count
849 of $CD4^+$ and $CD8^+$ T cells in the brain of healthy young and aged mice (n=8-13 mice, unpaired two-
850 tailed Student's t test after *arcsin* conversion).
851
852 **Supplementary Figure 2: OPC differentiation is impaired in the aged CNS. A** Representative images
853 of OLIG2 (cyan) and CC1 (magenta) in the healthy white matter of young and aged mice (scale bar =
854 50 µm). **B-D** Bar graph quantification showing $OLIG2^+$ oligodendrocyte lineage cell density,
855 $OLIG2^+CC1^+$ oligodendrocyte density and the proportion of differentiated oligodendrocytes in young
856 and aged healthy white matter (n=6-8 mice, unpaired two-tailed Student's t-test). **E** Representative
857 image of OLIG2 (cyan) and CC1 (magenta) immunostaining in lysolecithin-induced demyelinated
858 white matter of young and aged control mice (scale bar = 50 µm, lesion is demarcated by the white
859 dotted line). **F** Bar graph quantification showing $OLIG2^+CC1^+$ oligodendrocyte density in the
860 demyelinated lesion area in young and aged control mice (n=4 mice, unpaired two-tailed Student t-
861 test). **G, H** Bar graph quantification showing the density of $CD4^+$ T cells and $CD4^+Foxp3^+$ Treg in the
862 demyelinated area of young control and Treg expanded mice (n=3 mice, unpaired two-tailed
863 Student's t-test). **I, J** Bar graph quantification showing the density of $CD4^+$ T cells and $CD4^+Foxp3^+$

864 Treg in the demyelinated area of aged control and Treg expanded mice (n=6-7, unpaired two-tailed
865 Student's t-test).
866
867 **Supplementary Figure 3: Endogenous Treg depletion and reconstitution during lysolecithin-**
868 **induced demyelination *in vivo*. A** Gating strategy followed to identify natural Treg. **B** Bar graph
869 showing natural Treg isolation purity for *in vitro* experiments and *in vivo* adoptive transfer studies.
870 Natural Treg are identified by CD4 and CD25 expression (average 91% of the isolated cells for both
871 young and aged are $CD4^+CD25^+$) and by the expression of CD4 and Foxp3 (average 87% of the
872 isolated cells are positive for CD4 and Foxp3 in both young and aged mouse isolations) (n=14
873 independent isolations for different adoptive transfer rounds, each pool comprises 2-8 different
874 mice, Student's t test, after *arcsin* conversion). **C** Flow cytometric plot showing CD4 and GFP
875 expression to identify endogenous natural Treg in lymph nodes. **D** Bar graph showing quantification
876 for the proportion of endogenous GFP^+ Treg within the $CD4^+$ T cell population in the lymph nodes of
877 young Foxp3-DTR mice at 14dpl (n=7-9, 1-way ANOVA, after *arcsin* conversion, Sidak's multiple
878 comparisons test). **E** Flow cytometric plots showing CD25 and Foxp3 expression to detect Treg
879 reconstitution in lymph nodes after adoptive transfer. **F** Bar graph quantification shows the
880 proportion of $CD25^+Foxp3^+$ cells within the $CD4^+$ T cell population present in the lymph nodes of
881 young Foxp3-DTR mice at 14dpl (n=7-12, Kruskal Wallis and Dunn's multiple comparisons test). **G**
882 Representative images of immunostaining showing proliferating OPCs at 14 dpl (OLIG2 (green) and
883 Ki67 (magenta)) (scale bar = 100 µm, demyelinated area is indicated by the white line). **H-J** Bar graph
884 showing the areas of demyelination, the density of proliferating OPCs in the lesion and the
885 proportion of oligodendrocyte lineage cells proliferating in response to damage (n=7-8 mice, 1 way
886 ANOVA).
887
888 **Supplementary Figure. 4**: **A** Representative images of immunostaining for neurofilament-H (NFH,
889 green) and MBP (magenta) to quantify myelin wrapping as an early indicator of remyelination at 14

890 dpl (scale bar = 50 µm, demyelination area is highlighted by the white dotted line). **B-D**
891 Quantification shows the total number of axons, the density of MBP wrapped axons and the
892 percentage of MBP-wrapped axons from the total number of axons (n=4-6, 1-way ANOVA, Sidak's
893 multiple comparisons test). **E, F** Bar graph quantification showing reconstitution of $FOXP3^+$ Treg
894 within the $CD4^+$ population and the proportion of $CD25^+FOXP3^+$ Treg in $CD4^+$ T cells in the lymph
895 nodes of aged Foxp3-DTR at the point of sacrifice (n=4-7, Kruskal-Wallis, Dunn's multiple comparison
896 test).
897
898 **Supplementary Figure 5: Downstream analysis of differentially expressed genes between young**
899 **and aged natural Treg. A** Bar graphs showing the purity of young and aged natural Treg subjected to
900 RNA sequencing (on average 89% of $CD4^+$ cells were $Foxp3^+$, while 94% of $CD4^+$ cells were $CD25^+$)
901 (n=4-6 mice, Mann-Whitney U test). **B** Bar graph showing normalised counts of natural Treg marker
902 transcripts *Foxp3*, *Cd4* and *IL2ra*. **C** Heatmap of normalised count values of the Treg tissue repair
903 programme in male and female Treg. **D** Quantification of normalised count values of the Treg tissue
904 repair programme in male and female Treg. **E-G** Bar graphs showing the GO cellular component,
905 molecular function and KEGG pathways enriched within the differentially expressed genes
906 upregulated (magenta) and downregulated (purple) in aged Treg.
907
908 **Supplementary Figure 6: MCAM does not directly promote OPC differentiation. A, B** Bar graphs
909 showing the quantification of OPC differentiation in OPC and young Treg co-cultures in the presence
910 or absence of neutralising antibodies against candidate cell surface mediators, measured by the fold
911 change in the percentage of MBP^+ cells and the fold change in MBP^+ area per well (n=5-7, 2-way
912 ANOVA, Dunnet's multiple comparisons test). **C** Bar graph showing quantification of the proportion
913 of proliferating OPC ($Ki67^+$ cells) in rMCAM-treated neonatal OPCS at 6 days *in vitro* (n=7 mice, 2
914 independent experiments, 1-way ANOVA). **D** Bar graph showing quantification of the proportion of
915 proliferating OPC ($Ki67^+$ cells) in rITGA2-treated neonatal OPCS at 3 days *in vitro* (n=7 mice, 2

916 independent experiments, 1-way ANOVA, Dunnett's multiple comparison test). **E** Representative
917 images of immunostaining showing OPC differentiation in neonatal OPCs treated with recombinant
918 MCAM (OLIG2 (cyan), CNPase (grey) and MBP (magenta), scale bar = 50 µm). **F, G** Bar graphs
919 showing quantification of the proportion of MBP-expressing oligdoendrocytes and total MBP area
920 per well in rMCAM-treated neonatal OPCS at 6 days *in vitro* (n=7 mice, 2 independent experiments,
921 1-way ANOVA).
922
923 **Supplementary Figure 7: MCAM and ITGA2 levels are restored in aged Treg upon adoptive transfer**
924 **into young mice. A** Diagram explaining the experimental design of *in vivo* Treg depletion and RFP^+
925 Treg adoptive transfer. **B** Gating strategy for flow cytometric analyses**. C** Flow cytometric plots
926 showing MCAM expression in splenic RFP^+ Treg in control young and aged Foxp3-RFP mice and
927 young Foxp3-DTR mice that received young or aged RFP^+ cells (data shows 670 cells from the
928 concatenation of 2-3 mice in each). **D** Bar graph quantification of the proportion of $MCAM^+$ cells
929 within RFP population (n=2-3 mice, no statistical analysis performed). **E** Bar graph showing the
930 median fluorescent intensity of MCAM in $MCAM^+RFP^+$ cells (n=2-3 mice, no statistical analysis
931 performed). **F** Flow cytometric plots showing ITGA2 expression in splenic RFP^+ Treg in control young
932 and aged Foxp3-RFP mice and young Foxp3-DTR mice that received young or aged RFP^+ cells (data
933 shows 670 cells from the concatenation of 2-3 mice in each). **G** Bar graph quantification of the
934 proportion of $ITGA2^+$ cells within RFP population (n=2-3 mice, no statistical analysis performed). **H**
935 Bar graph showing the median fluorescent intensity of ITGA2 in $MCAM^+RFP^+$ cells (n=2-3 mice, no
936 statistical analysis performed). statistical analysis performed).
937
938
939 **Supplementary Table 1:** Statistical analysis of the differentially expressed genes between young and
940 aged Treg. Related to Fig. 6 and Sup. Fig. 5.
941

Acknowledgements

We acknowledge extensive technical support from Carmel McVicar, Maria P Athanasios, Michelle Naughton and the staff of the animal facility. We thank A. Rudensky (Memorial Sloan Kettering Cancer Centre) for providing Foxp3-DTR mice. We thank the laboratory of Anna Williams (University of Edinburgh) for the Fiji plug-in to analyse myelination index in brain slice cultures.

This work was supported by the Wellcome Trust (110138/Z/15/Z to DCF), Biotechnology and Biological Sciences Research Council (BB/J01026X/1 and BB/N003721/1, to DCF), ECTRIMS postdoctoral fellowship (to AGF), Wellcome ISSF fellowship (to AGF), Miguel Servet Fellowship from the Spanish Institute of Health Carlos III (CP21/00032 to AGF), Spanish State Research Agency Plan Generación de Conocimiento 2021 grant (PID2021-124465OA-I00 to AGF), The Leverhulme Trust (ECF-2014-390, to YD), a postdoctoral fellowship contract from the Generalitat Valenciana (APOSTD21, to FJR and postgraduate studentship support from the Dept. for the Economy (Northern Ireland).

Author contributions

Experiments were designed by A.G.F., D.C.F., A.L., R.J.M, J.D Y.D. and V.T. Experiments were performed and/or analysed by A.G.F., M.D., E.H., N.V.G., J.W., A.Y., K.M., J.F., S.C.F., T.M., A.D., F.J.R.B., K.S.R., C.E.M., M.I., J.D., R.P., Y.D. and D.C.F. A.L, R.J.I, R.J.M and C.E.M. provided advice on experimental design and interpretation. Manuscript was written by A.G.F. and D.C.F. with contributions from all authors. D.C.F and A.G.F. oversaw the study.

References

1. Nave, K.-A. & Werner, H. B. Ensheathment and Myelination of Axons: Evolution of Glial Functions. *Annu Rev Neurosci* **44**, 197-219 (2021).

968 2. Griffiths, I. *et al.* Axonal swellings and degeneration in mice lacking the major proteolipid of
969 myelin. *Science* **280**, 1610–1613 (1998).

970 3. Lappe-Siefke, C. *et al.* Disruption of Cnp1 uncouples oligodendroglial functions in axonal support
971 and myelination. *Nat Genet* **33**, 366–374 (2003).

972 4. Love, S. Demyelinating diseases. *J Clin Pathol* **59**, 1151-9 (2006).

973 5. Bodini, B. *et al.* Dynamic Imaging of Individual Remyelination Profiles in Multiple Sclerosis. *Ann*
974 *Neurol* **79**, 726–738 (2016).

975 6. Franklin, R. J. M. & ffrench-Constant, C. Regenerating CNS myelin — from mechanisms to
976 experimental medicines. *Nat Rev Neurosci* **18**, 753–769 (2017).

977 7. MD, P. C. L., MD, B. Z., MD, P. A. W., MD, P. C. S. & MD, P. B. S. Remyelination in multiple sclerosis:
978 from basic science to clinical translation. *Lancet* **19**, 678–688 (2020).

979 8. Ricigliano, V. A. G. *et al.* Spontaneous remyelination in lesions protects the integrity of
980 surrounding tissues over time in multiple sclerosis. *Eur. J. Neurol.* **29**, 1719–1729 (2022).

981 9. Shields, S., Gilson, J., Blakemore, W. & Franklin, R. Remyelination occurs as extensively but more
982 slowly in old rats compared to young rats following fliotoxin-induced CNS demyelination. *Glia* **29**,
983 1098-1136 (2000).

984 10. Sim, F. J., Zhao, C., Penderis, J. & Franklin, R. J. M. The age-related decrease in CNS remyelination
985 efficiency is attributable to an impairment of both oligodendrocyte progenitor recruitment and
986 differentiation. *Journal of Neuroscience* **22**, 2451–2459 (2002).

987 11. McMurran, C. E. *et al.* Remyelination in humans due to a retinoid-X receptor agonist is
988 age-dependent. *Ann Clin Transl Neur* **9**, 1090-1094 (2022)

989 12. Confavreux, C. & Vukusic, S. Age at disability milestones in multiple sclerosis. *Brain* **129**, 595–605
990 (2006).

991 13. Neumann, B. *et al.* Metformin Restores CNS Remyelination Capacity by Rejuvenating Aged Stem
992 Cells. *Cell Stem Cell* **25**, 473-485.e8 (2019).

993 14. Fuente, A. G. de la *et al.* Changes in the Oligodendrocyte Progenitor Cell Proteome with Ageing.
994 *Mol. Cell. Proteom.* **19**, 1281–1302 (2020).

995 15. Spitzer, S. O. *et al.* Oligodendrocyte Progenitor Cells Become Regionally Diverse and
996 Heterogeneous with Age. *Neuron* **101**, 459-471 (2019).

997 16. Baror, R. *et al.* Transforming growth factor-beta renders ageing microglia inhibitory to
998 oligodendrocyte generation by CNS progenitors. *Glia* **37**, 2409–11 (2019).

999 17. Segel, M. *et al.* Niche stiffness underlies the ageing of central nervous system progenitor cells.
1000 *Nature* **350**, 1199–134 (2019).

1001 18. Ruckh, J. M. *et al.* Rejuvenation of regeneration in the aging central nervous system. *Cell stem*
1002 *cell* **10**, 96–103 (2012).

1003 19. Natrajan, M. S. *et al.* Retinoid X receptor activation reverses age-related deficiencies in myelin
1004 debris phagocytosis and remyelination. *Brain* **138**, 3581–3597 (2015).

1005 20. Cantuti-Castelvetri, L. *et al.* Defective cholesterol clearance limits remyelination in the aged
1006 central nervous system. *Science* **359**, 684-688 (2018).

1007 21. McNamara, N. B. *et al.* Microglia regulate central nervous system myelin growth and integrity.
1008 *Nature* 613, 120-129 (2022).

1009 22. Rawji, K. S., Neumann, B. & Franklin, R. J. M. Glial aging and its impact on central nervous system
1010 myelin regeneration. *Ann Ny Acad Sci* **1519**, 34-45 (2022).

1011 23. Rawji, K. S., Martinez, G. A. G., Sharma, A. & Franklin, R. J. M. The Role of Astrocytes in
1012 Remyelination. *Trends in neurosciences* **43**, 596–607 (2020).

1013 24. Franklin, R. J. M., ffrench-Constant, C., Edgar, J. M. & Smith, K. J. Neuroprotection and repair in
1014 multiple sclerosis. *Nature Reviews Neurology* **8**, 624–634 (2012).

1015 25. Burzyn, D. *et al.* A special population of regulatory T cells potentiates muscle repair. *Cell* **155**,
1016 1282–1295 (2013).

1017 26. Ali, N. *et al.* Regulatory T Cells in Skin Facilitate Epithelial Stem Cell Differentiation. *Cell* **169**,
1018 1119-1123.e11 (2017).

1019 27. Dombrowski, Y. *et al.* Regulatory T cells promote myelin regeneration in the central nervous
1020 system. *Nat Neurosci* **20**, 674–680 (2017).

1021 28. McIntyre, L. L. *et al.* Regulatory T cells promote remyelination in the murine experimental
1022 autoimmune encephalomyelitis model of multiple sclerosis following human neural stem cell
1023 transplant. *Neurobiology of Disease* **140**, 104868 (2020).

1024 29. Shi, L. *et al.* Treg cell-derived osteopontin promotes microglia-mediated white matter repair
1025 after ischemic stroke. *Immunity* **54**, 1527-1542.e8 (2021).

1026 30. Garg, S. K. *et al.* Aging is associated with increased regulatory T-cell function. *Aging Cell* **13**, 441–
1027 448 (2014).

1028 31. Elyahu, Y. *et al.* Aging promotes reorganization of the CD4 T cell landscape toward extreme
1029 regulatory and effector phenotypes. *Sci adv* **5**, eaaw8330 (2019).

1030 32. Dulken, B. W. *et al.* Single-cell analysis reveals T cell infiltration in old neurogenic niches. *Nature*
1031 **571**, 205–210 (2019).

1032 33. Kaya, T. *et al.* CD8+ T cells induce interferon-responsive oligodendrocytes and microglia in white
1033 matter aging. *Nat Neurosci* **25**, 1446–1457 (2022).

1034 34. Groh, J. *et al.* Accumulation of cytotoxic T cells in the aged CNS leads to axon degeneration and
1035 contributes to cognitive and motor decline. *Nat Aging* **1**, 357-367 (2021).

1036 35. Pasciuto, E. *et al.* Microglia Require CD4 T Cells to Complete the Fetal-to-Adult Transition. *Cell*
1037 **182**, 625-640 (2020).

1038 36. Kuswanto, W. *et al.* Poor Repair of Skeletal Muscle in Aging Mice Reflects a Defect in Local,
1039 Interleukin-33-Dependent Accumulation of Regulatory T Cells. *Immunity* **44**, 355–367 (2016).

1040 37. Ximerakis, M. *et al.* Single-cell transcriptomic profiling of the aging mouse brain. *Nature Neurosci*
1041 **22**, 1696-1708 (2019).

1042 38. Allen, W. E., Blosser, T. R., Sullivan, Z. A., Dulac, C. & Zhuang, X. Molecular and spatial signatures
1043 of mouse brain aging at single-cell resolution. *Cell* **186**, 194-208(2022).

1044 39. McMurran, C. E., Zhao, C. & Franklin, R. J. M. Toxin-Based Models to Investigate Demyelination
1045 and Remyelination. *Methods Mol. Biol. (Clifton, NJ)* **1936**, 377–396 (2019).

1046 40. Dittmer, M. *et al.* Characterization of a murine mixed neuron-glia model and cellular responses
1047 to regulatory T cell-derived factors. *Molec brain* **11**, 25 (2018).

1048 41. Zhang, H., Jarjour, A. A., Boyd, A. & Williams, A. Central nervous system remyelination in culture
1049 — A tool for multiple sclerosis research. *Expl Neurol* **230**, 138–148 (2011).

1050 42. Kim, J. M., Rasmussen, J. P. & Rudensky, A. Y. Regulatory T cells prevent catastrophic
1051 autoimmunity throughout the lifespan of mice. *Nat Immunol* **8**, 191–197 (2007).

1052 43. Guo, Z. *et al.* DCAF1 regulates Treg senescence via the ROS axis during immunological ageing. *J*
1053 *Clin Invest* **130**, 5893–5908 (2020).

1054 44. Morales-Nebreda, L. *et al.* Aging imparts cell-autonomous dysfunction to regulatory T cells
1055 during recovery from influenza pneumonia. *JCI Insight* **6**, e141690 (2021).

1056 45. Delacher, M. *et al.* Single-cell chromatin accessibility landscape identifies tissue repair program in
1057 human regulatory T cells. *Immunity* **54**, 702-720 (2021).

1058 46. Zhang, Y. *et al.* An RNA-sequencing transcriptome and splicing database of glia, neurons, and
1059 vascular cells of the cerebral cortex. *J Neurosci* **34**, 11929–11947 (2014).

1060 47. Jensen, L. J. *et al.* STRING 8--a global view on proteins and their functional interactions in 630
1061 organisms. *Nucleic Acids Res* **37**, D412-6 (2009).

1062 48. Linehan, E. *et al.* Aging impairs peritoneal but not bone marrow-derived macrophage
1063 phagocytosis. *Aging cell* **13**, 699–708 (2014).

1064 49. Wang, W., Thomas, R., Oh, J. & Su, D. Accumulation of pTreg cells is detrimental in late-onset
1065 (aged) mouse model of multiple sclerosis. *Aging Cell* **21**, e13630 (2022).

1066 50. Louapre, C. *et al.* A randomized double-blind placebo-controlled trial of low-dose interleukin-2 in
1067 relapsing–remitting multiple sclerosis. *J. Neurol.* **270**, 4403–4414 (2023).

1068 51. Muñoz-Rojas, A. R. & Mathis, D. Tissue regulatory T cells: regulatory chameleons. *Nat Rev*
1069 *Immunol* **21**, 597-611 (2021).

1070 52. Laursen, L. S., Chan, C. W. & ffrench-Constant, C. An Integrin-Contactin Complex Regulates CNS
1071 Myelination by Differential Fyn Phosphorylation. *J Neurosci* **29**, 9174–9185 (2009).

1072 53. Breuer, J. *et al.* Blockade of MCAM/CD146 impedes CNS infiltration of T cells over the choroid
1073 plexus. *J Neuroinflamm* **15**, 236 (2018).

1074 54. Zondler, L. *et al.* MCAM/CD146 Signaling via PLCγ1 Leads to Activation of β1-Integrins in Memory
1075 T-Cells Resulting in Increased Brain Infiltration. *Front Immunol* **11**, 599936 (2020).

1076 55. Larochelle, C. *et al.* Melanoma cell adhesion molecule–positive CD8 T lymphocytes mediate
1077 central nervous system inflammation. *Ann Neurol.* **78**, 39–53 (2015).

1078 56. Olajuyin, A. M., Olajuyin, A. K., Wang, Z., Zhao, X. & Zhang, X. CD146 T cells in lung cancer: its
1079 function, detection, and clinical implications as a biomarker and therapeutic target. *Cancer Cell Int.*
1080 **19**, 247 (2019).

1081 57. Şeftalioğlu, A. & Karakoç, L. Expression of CD146 adhesion molecules (MUC18 or MCAM) in the
1082 thymic microenvironment. *Acta Histochem.* **102**, 69–83 (2000).

1083 58. Yshii, L. *et al.* Astrocyte-targeted gene delivery of interleukin 2 specifically increases brain-
1084 resident regulatory T cell numbers and protects against pathological neuroinflammation. *Nat*
1085 *Immunol* **23**, 878–891 (2022).

1086 59. Webster, K. E. *et al.* In vivo expansion of T reg cells with IL-2–mAb complexes: induction of
1087 resistance to EAE and long-term acceptance of islet allografts without immunosuppression. *J Exp*
1088 *Medicine* **206**, 751–760 (2009).

1089 60. Schindelin, J. *et al.* Fiji: an open-source platform for biological-image analysis. *Nat Methods* **9**,
1090 676–682 (2012).

1091 61. Stirling, D. R. *et al.* CellProfiler 4: improvements in speed, utility and usability. *BMC*
1092 *Bioinformatics* **22**, 433 (2021).

1093 62. Dao, D. *et al.* CellProfiler Analyst: interactive data exploration, analysis and classification of large
1094 biological image sets. *Bioinformatics* **32**, 3210–3212 (2016).

1095 63. Martin, M. Cutadapt removes adapter sequences from high-throughput sequencing reads.
1096 *Embnet J* **17**, 10–12 (2011).

1097 64. Dobin, A. *et al.* STAR: ultrafast universal RNA-seq aligner. *Bioinformatics* **29**, 15–21 (2013).

1098 65. Liao, Y., Smyth, G. K. & Shi, W. featureCounts: an efficient general purpose program for assigning
1099 sequence reads to genomic features. *Bioinformatics* **30**, 923–930 (2013).

1100 66. Love, M. I., Huber, W. & Anders, S. Moderated estimation of fold change and dispersion for RNA-
1101 seq data with DESeq2. *Genome Biol* **15**, 550 (2014).

1102

1103

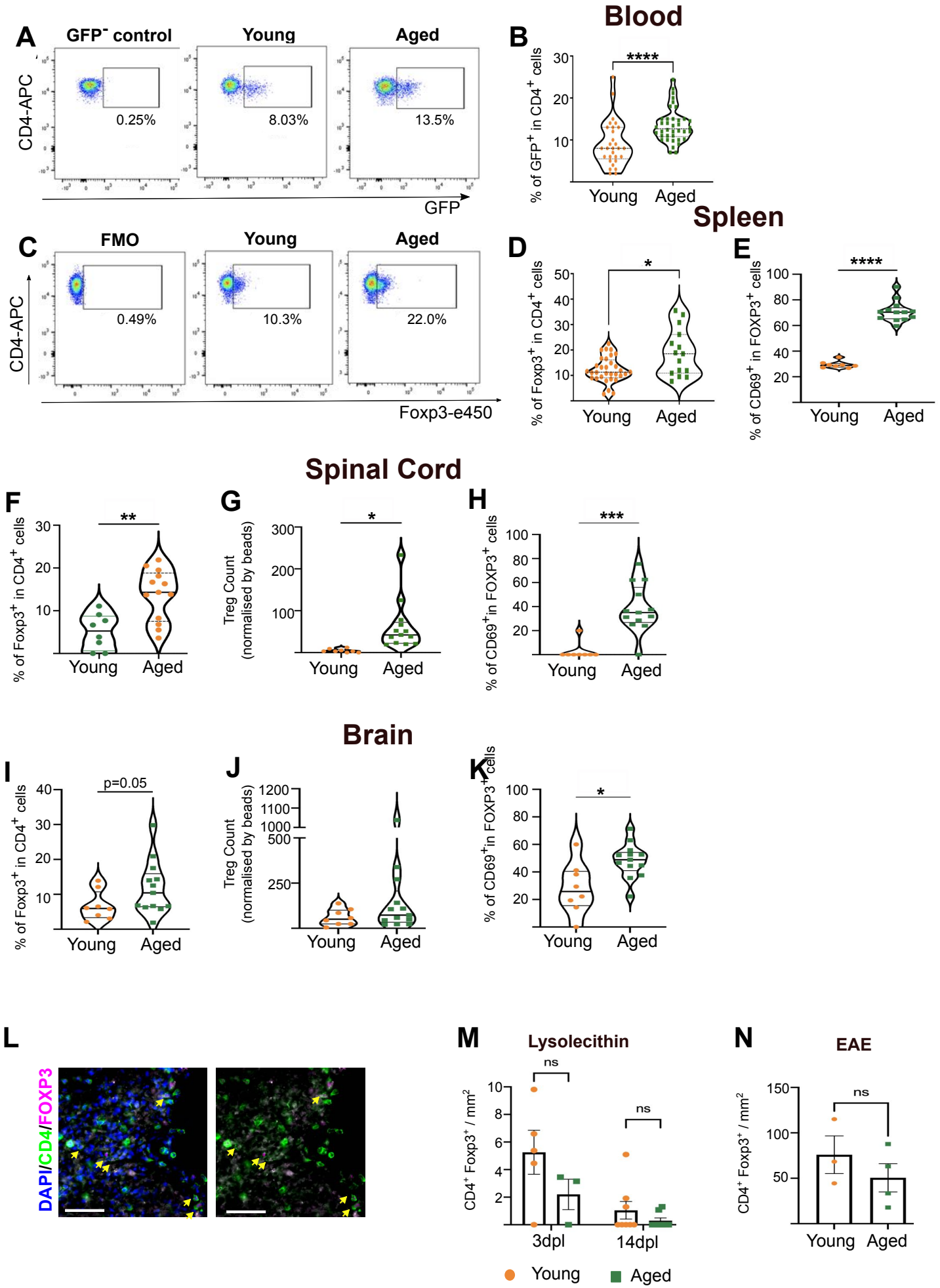
A
GFP⁻ control
Young
Aged
CD4-APC
0.25%
8.03%
13.5%
GFP
B
Blood
% of GFP+ in CD4+ cells
****
Young
Aged
C
FMO
Young
Aged
CD4-APC
0.49%
10.3%
22.0%
Foxp3-e450
D
Spleen
% of Foxp3+ in CD4+ cells
*
Young
Aged
E
% of CD69+ in FOXP3+ cells
****
Young
Aged
Spinal Cord
F
% of Foxp3+ in CD4+ cells
**
Young
Aged
G
Treg Count (normalised by beads)
*
Young
Aged
H
% of CD69+ in FOXP3+ cells
***
Young
Aged
Brain
I
% of Foxp3+ in CD4+ cells
p=0.05
Young
Aged
J
Treg Count (normalised by beads)
Young
Aged
K
% of CD69+ in FOXP3+ cells
*
Young
Aged
L
DAPI/CD4/FOXP3
M
Lysolecithin
CD4+ Foxp3+ / mm2
ns
ns
3dpl
14dpl
Young
Aged
N
EAE
CD4+ Foxp3+ / mm2
ns
Young
Aged

Fig. 1

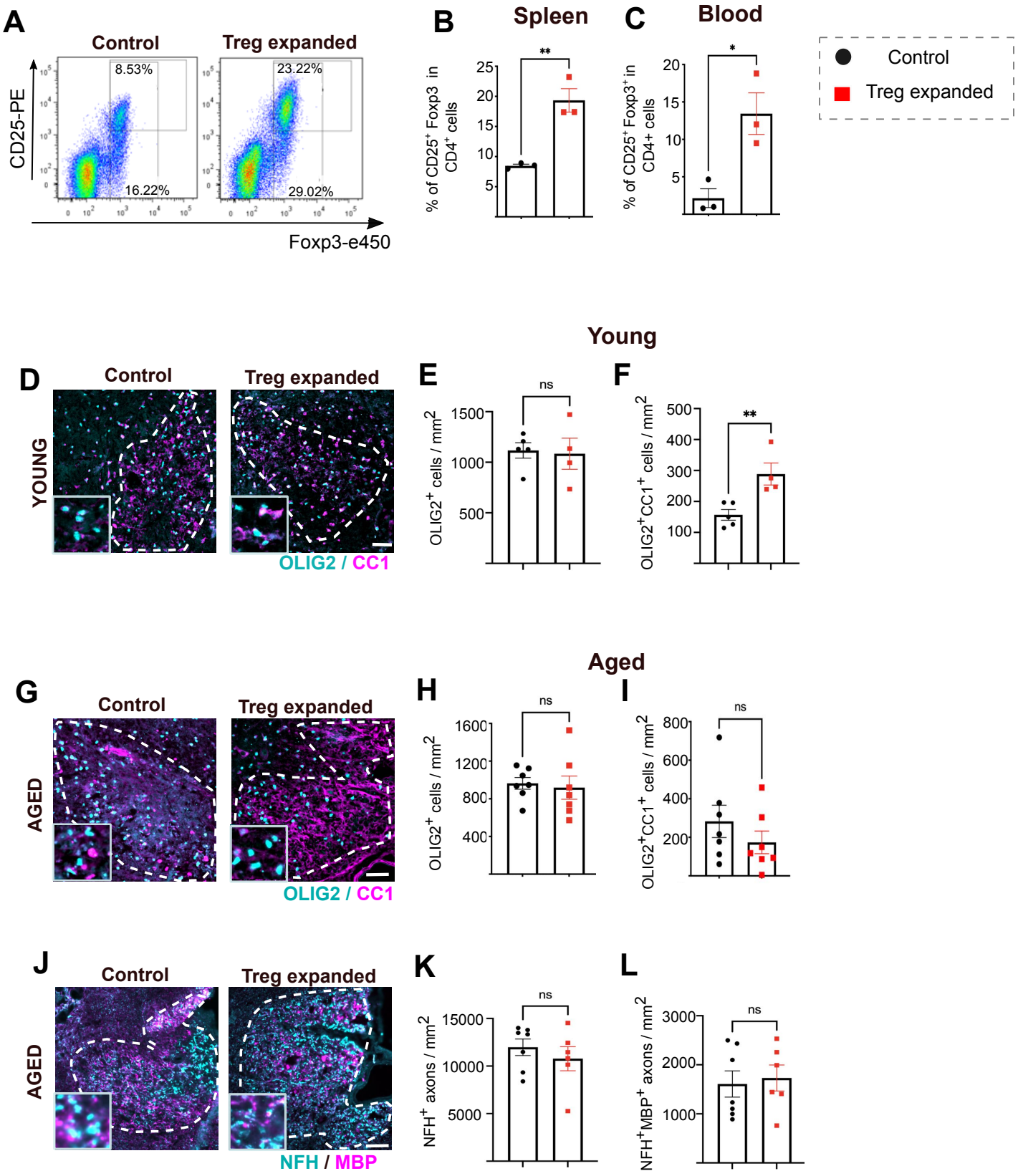
A
Control
Treg expanded
8.53%
16.22%
23.22%
29.02%
CD25-PE
Foxp3-e450
B
Spleen
% of CD25+ Foxp3 in CD4+ cells
**
C
Blood
% of CD25+ Foxp3+ in CD4+ cells
*
Control
Treg expanded
Young
D
Control
Treg expanded
YOUNG
OLIG2 / CC1
E
OLIG2+ cells / mm2
ns
F
OLIG2+CC1+ cells / mm2
**
Aged
G
Control
Treg expanded
AGED
OLIG2 / CC1
H
OLIG2+ cells / mm2
ns
I
OLIG2+CC1+ cells / mm2
ns
J
Control
Treg expanded
AGED
NFH / MBP
K
NFH+ axons / mm2
ns
L
NFH+MBP+ axons / mm2
ns

Fig. 2

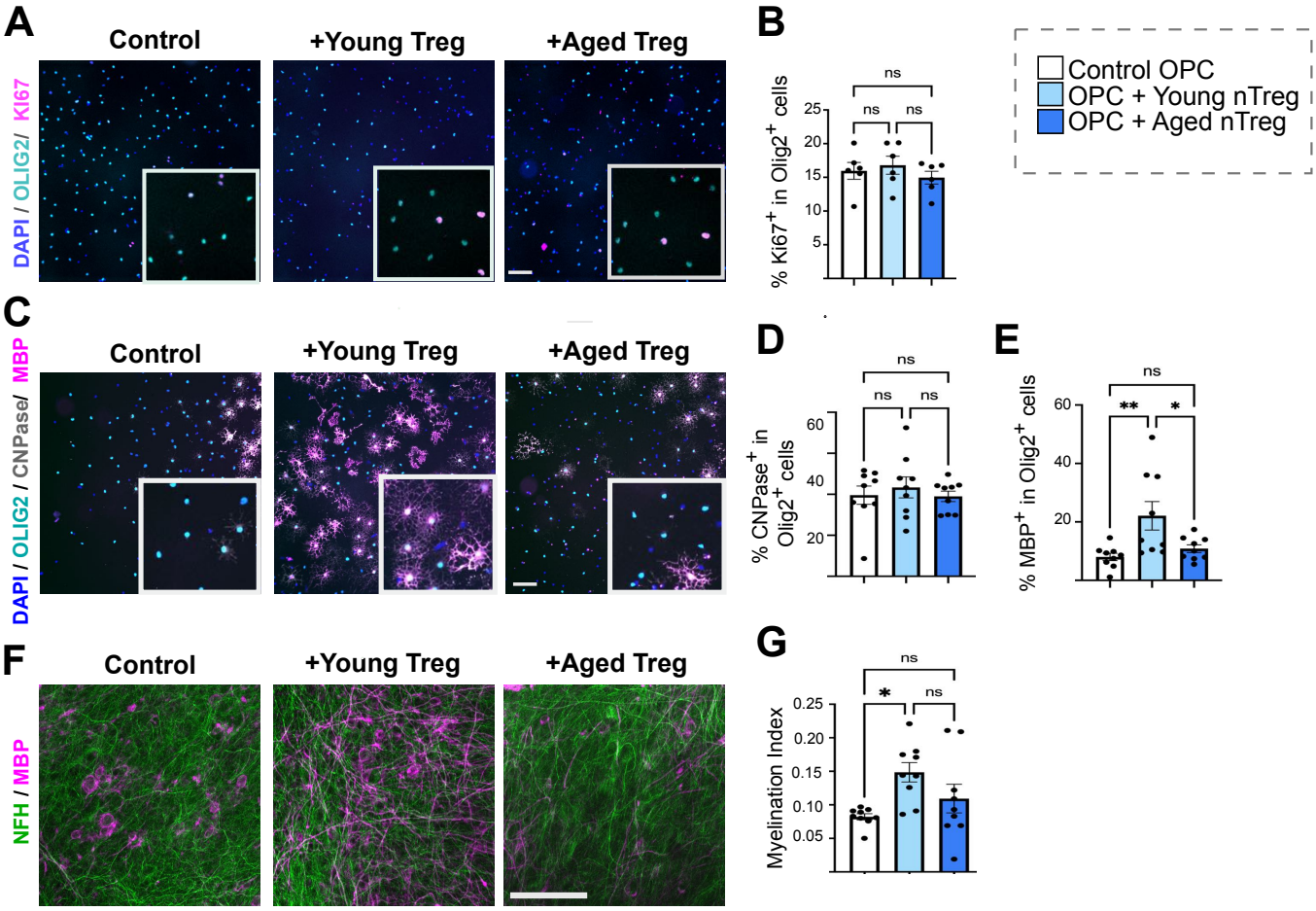
A
Control
+Young Treg
+Aged Treg
DAPI / OLIG2/ Ki67
B
% Ki67+ in Olig2+ cells
ns
ns
ns
Control OPC
OPC + Young nTreg
OPC + Aged nTreg
C
Control
+Young Treg
+Aged Treg
DAPI / OLIG2 / CNPase/ MBP
D
% CNPase+ in Olig2+ cells
E
% MBP+ in Olig2+ cells
**
*
F
Control
+Young Treg
+Aged Treg
NFH / MBP
G
Myelination Index
*

Fig. 3

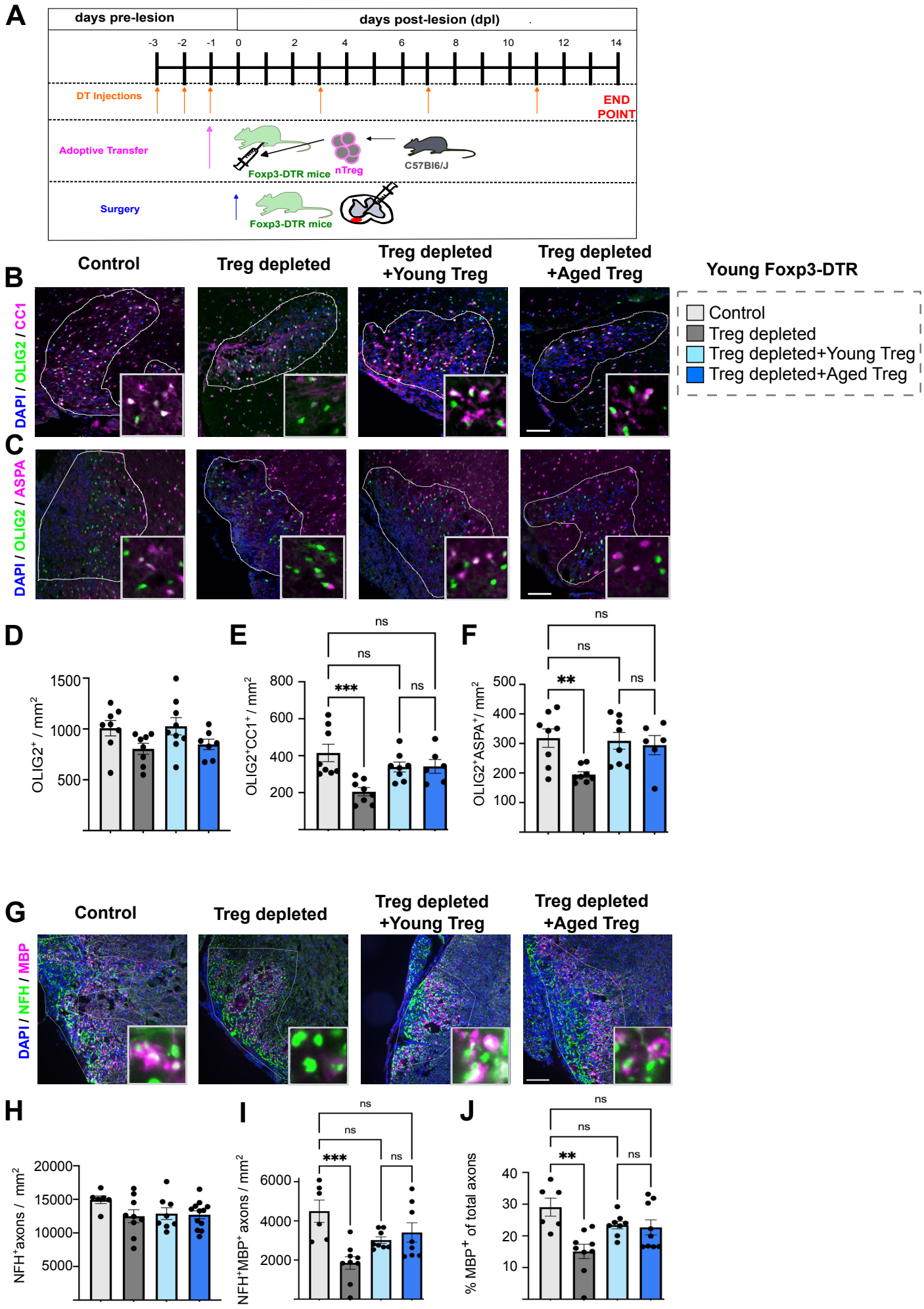
A
days pre-lesion
days post-lesion (dpl)
-3 -2 -1 0 2 4 6 8 10 12 14
DT Injections
END POINT
Adoptive Transfer
Foxp3-DTR mice
nTreg
C57Bl6/J
Surgery
Foxp3-DTR mice
B
Control
Treg depleted
Treg depleted +Young Treg
Treg depleted +Aged Treg
Young Foxp3-DTR
Control
Treg depleted
Treg depleted+Young Treg
Treg depleted+Aged Treg
DAPI / OLIG2 / CC1
C
DAPI / OLIG2 / ASPA
D
OLIG2+ / mm2
1500
1000
500
E
OLIG2+CC1+ / mm2
800
600
400
200
ns
ns
***
ns
F
OLIG2+ASPA+/ mm2
500
400
300
200
100
ns
ns
**
ns
G
Control
Treg depleted
Treg depleted +Young Treg
Treg depleted +Aged Treg
DAPI / NFH / MBP
H
NFH+axons / mm2
20000
15000
10000
5000
I
NFH+MBP+ axons / mm2
6000
4000
2000
ns
ns
***
ns
J
% MBP+ of total axons
40
30
20
10
ns
ns
**
ns

Fig. 4

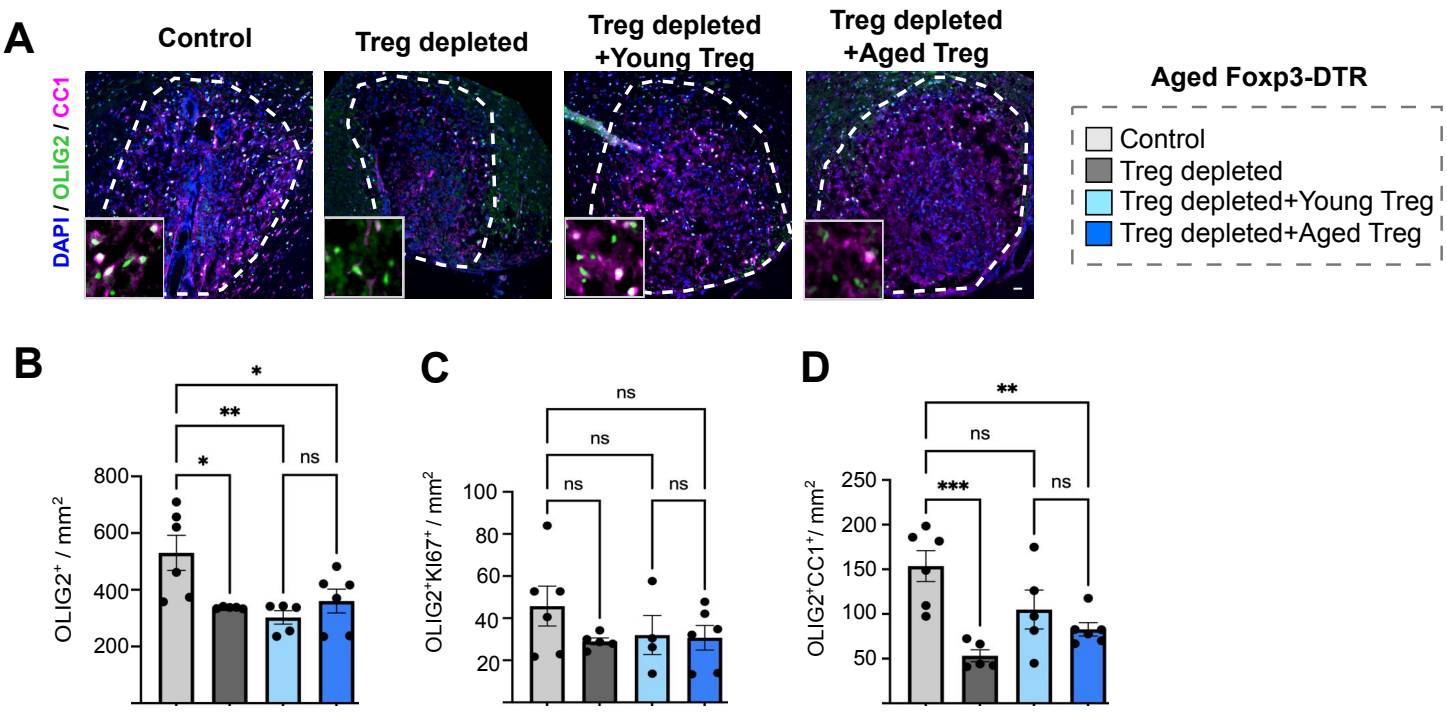
A
Control
Treg depleted
Treg depleted +Young Treg
Treg depleted +Aged Treg
DAPI / OLIG2 / CC1
Aged Foxp3-DTR
Control
Treg depleted
Treg depleted+Young Treg
Treg depleted+Aged Treg
B
OLIG2+ / mm2
800
600
400
200
*
**
*
ns
C
OLIG2+KI67+ / mm2
100
80
60
40
20
ns
ns
ns
ns
D
OLIG2+CC1+/ mm2
250
200
150
100
50
**
ns
***
ns

Fig. 5

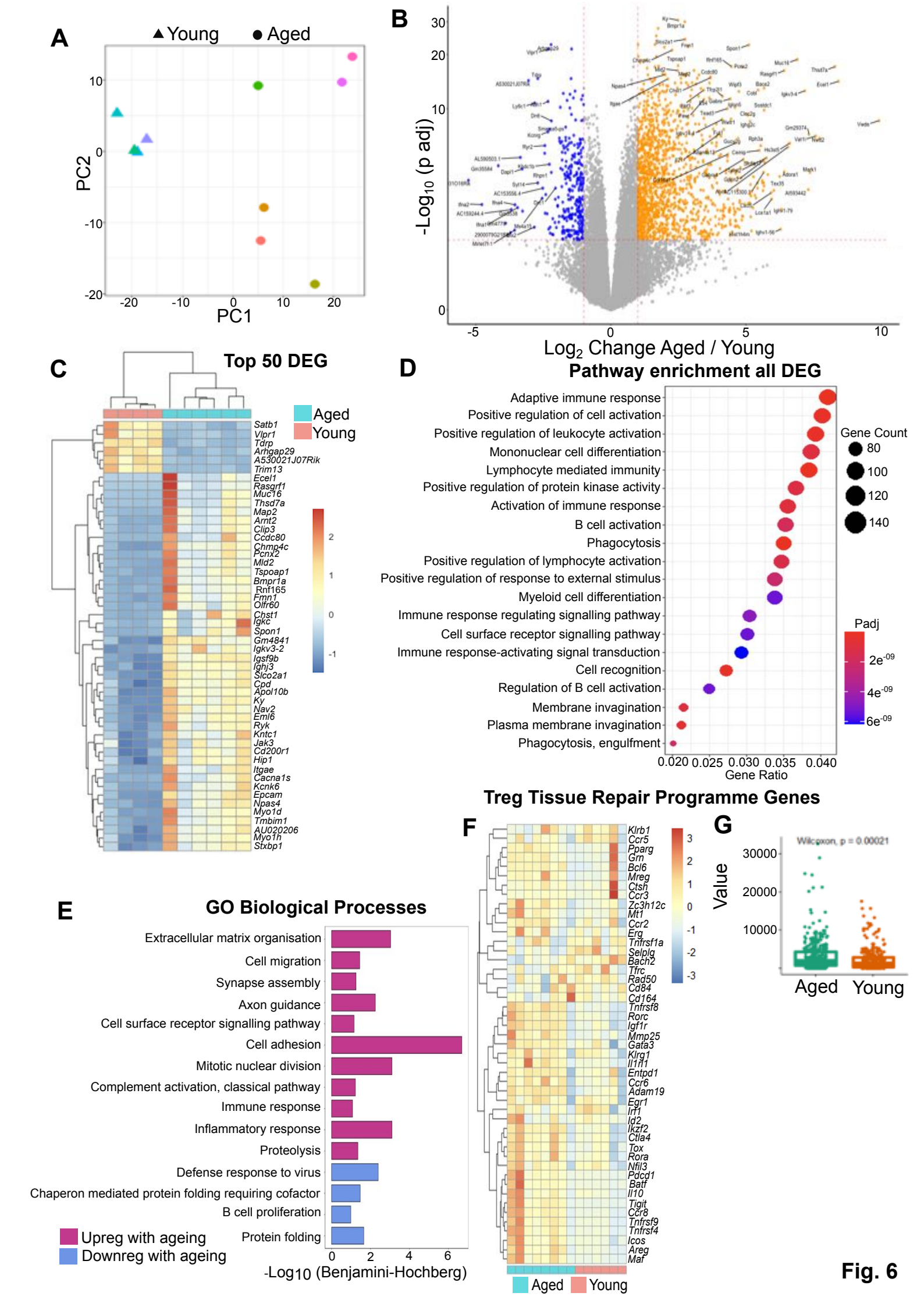
A
Young
Aged
PC2
PC1
B
-Log10 (p adj)
Log2 Change Aged / Young
C
Top 50 DEG
Aged
Young
Satb1
Vlpr1
Tdrp
Arhgap29
A530021J07Rik
Trim13
Ecel1
Rasgrf1
Muc16
Thsd7a
Map2
Arnt2
Clip3
Ccdc80
Chmp4c
Pcnx2
Mld2
Tspoap1
Bmpr1a
Rnf165
Fmn1
Olfr60
Chst1
Igkc
Spon1
Gm4841
Igkv3-2
Igsf9b
Ighj3
Slco2a1
Cpd
Apol10b
Ky
Nav2
Eml6
Ryk
Kntc1
Jak3
Cd200r1
Hip1
Itgae
Cacna1s
Kcnk6
Epcam
Npas4
Myo1d
Tmbim1
AU020206
Myo1h
Stxbp1
D
Pathway enrichment all DEG
Adaptive immune response
Positive regulation of cell activation
Positive regulation of leukocyte activation
Mononuclear cell differentiation
Lymphocyte mediated immunity
Positive regulation of protein kinase activity
Activation of immune response
B cell activation
Phagocytosis
Positive regulation of lymphocyte activation
Positive regulation of response to external stimulus
Myeloid cell differentiation
Immune response regulating signalling pathway
Cell surface receptor signalling pathway
Immune response-activating signal transduction
Cell recognition
Regulation of B cell activation
Membrane invagination
Plasma membrane invagination
Phagocytosis, engulfment
Gene Ratio
Gene Count
Padj
E
GO Biological Processes
Extracellular matrix organisation
Cell migration
Synapse assembly
Axon guidance
Cell surface receptor signalling pathway
Cell adhesion
Mitotic nuclear division
Complement activation, classical pathway
Immune response
Inflammatory response
Proteolysis
Defense response to virus
Chaperon mediated protein folding requiring cofactor
B cell proliferation
Protein folding
Upreg with ageing
Downreg with ageing
-Log10 (Benjamini-Hochberg)
Treg Tissue Repair Programme Genes
F
Klrb1
Ccr5
Pparg
Grn
Bcl6
Mreg
Ctsh
Ccr3
Zc3h12c
Mt1
Ccr2
Erg
Tnfrsf1a
Selplg
Bach2
Tfrc
Rad50
Cd84
Cd164
Tnfrsf8
Rorc
Igf1r
Mmp25
Gata3
Klrg1
Il1rl1
Entpd1
Ccr6
Adam19
Egr1
Irf1
Id2
Ikzf2
Ctla4
Tox
Rora
Nfil3
Pdcd1
Batf
Il10
Tigit
Ccr8
Tnfrsf9
Tnfrsf4
Icos
Areg
Maf
Aged
Young
G
Wilcoxon, p = 0.00021
Value
Aged
Young
Fig. 6

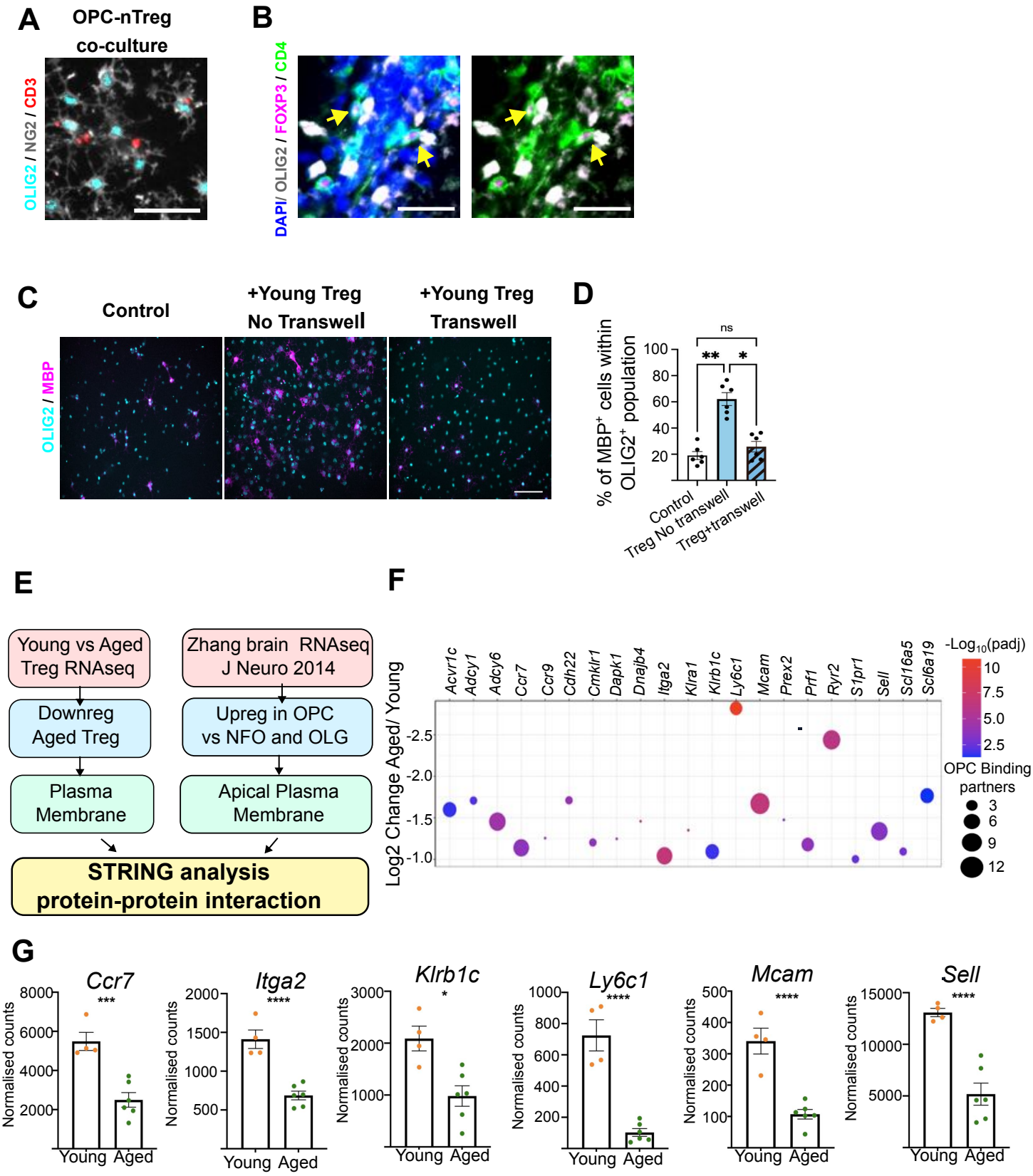
A
OPC-nTreg co-culture
OLIG2 / NG2 / CD3
B
DAPI/ OLIG2 / FOXP3 / CD4
C
Control
+Young Treg No Transwell
+Young Treg Transwell
OLIG2 / MBP
D
% of MBP+ cells within OLIG2+ population
ns
**
*
Control
Treg No transwell
Treg+transwell
E
Young vs Aged Treg RNAseq
Downreg Aged Treg
Plasma Membrane
Zhang brain RNAseq J Neuro 2014
Upreg in OPC vs NFO and OLG
Apical Plasma Membrane
STRING analysis protein-protein interaction
F
Log2 Change Aged/ Young
Acvr1c
Adcy1
Adcy6
Ccr7
Ccr9
Cdh22
Cmklr1
Dapk1
Dnajb4
Itga2
Klra1
Klrb1c
Ly6c1
Mcam
Prex2
Prf1
Ryr2
S1pr1
Sell
Scl16a5
Scl6a19
-Log10(padj)
OPC Binding partners
G
Ccr7
Itga2
Klrb1c
Ly6c1
Mcam
Sell
Normalised counts
Young
Aged

Fig. 7

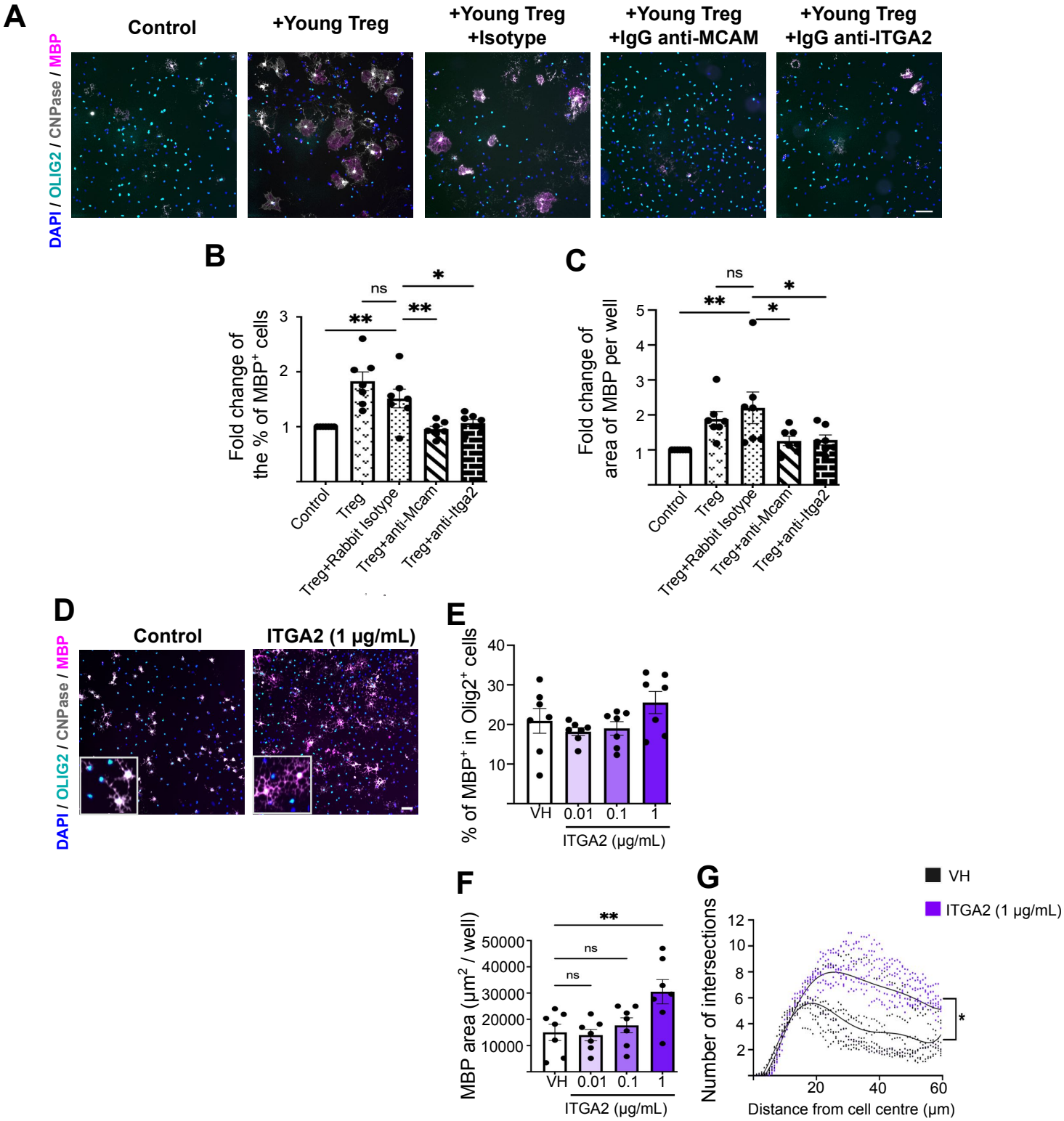
A
Control
+Young Treg
+Young Treg +Isotype
+Young Treg +IgG anti-MCAM
+Young Treg +IgG anti-ITGA2
DAPI / OLIG2 / CNPase / MBP
B
Fold change of the % of MBP+ cells
ns
**
**
*
Control
Treg
Treg+Rabbit Isotype
Treg+anti-Mcam
Treg+anti-Itga2
C
Fold change of area of MBP per well
ns
**
*
*
D
Control
ITGA2 (1 µg/mL)
DAPI / OLIG2 / CNPase / MBP
E
% of MBP+ in Olig2+ cells
VH
0.01
0.1
1
ITGA2 (µg/mL)
F
MBP area (µm2 / well)
**
ns
ns
ITGA2 (µg/mL)
G
VH
ITGA2 (1 µg/mL)
Number of intersections
Distance from cell centre (µm)
*

Fig. 8

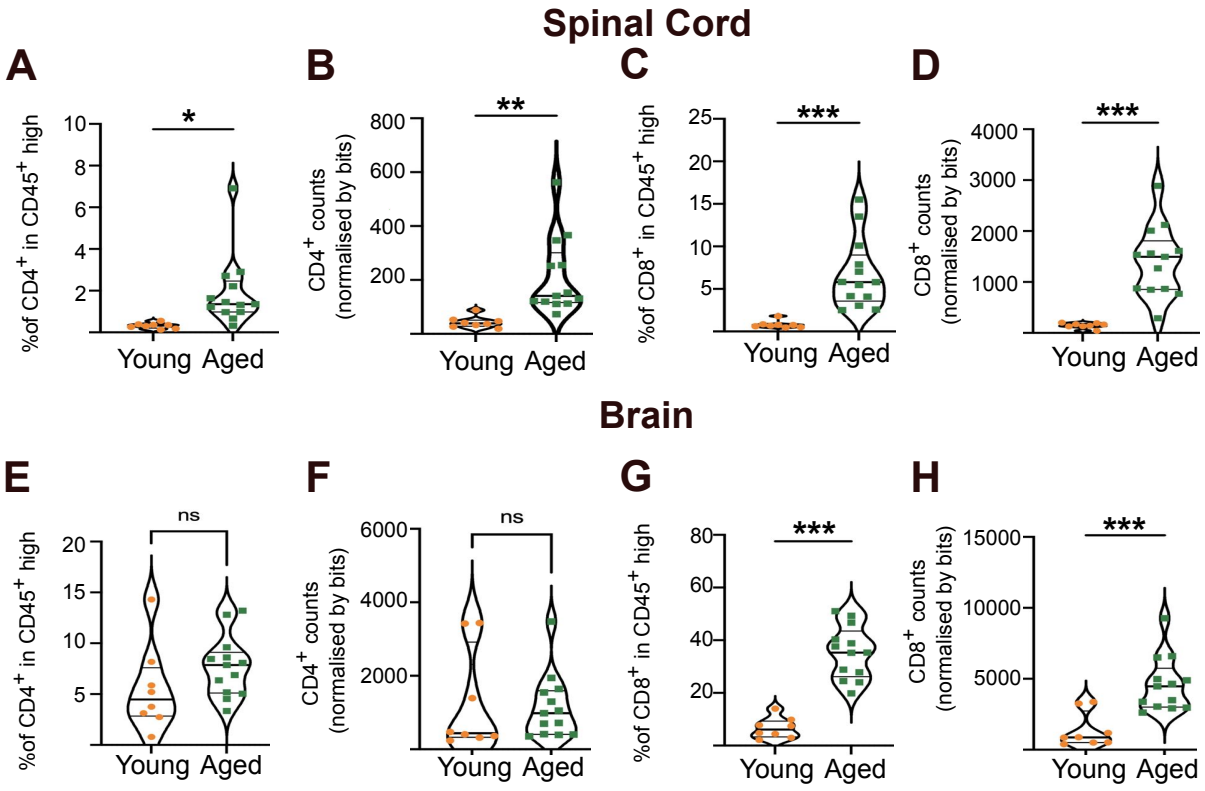
Spinal Cord
A
B
C
D
%of CD4+ in CD45+ high
CD4+ counts (normalised by bits)
%of CD8+ in CD45+ high
CD8+ counts (normalised by bits)
Young
Aged
*
**
***
***
Brain
E
F
G
H
ns
ns
***
***

Sup. Fig. 1

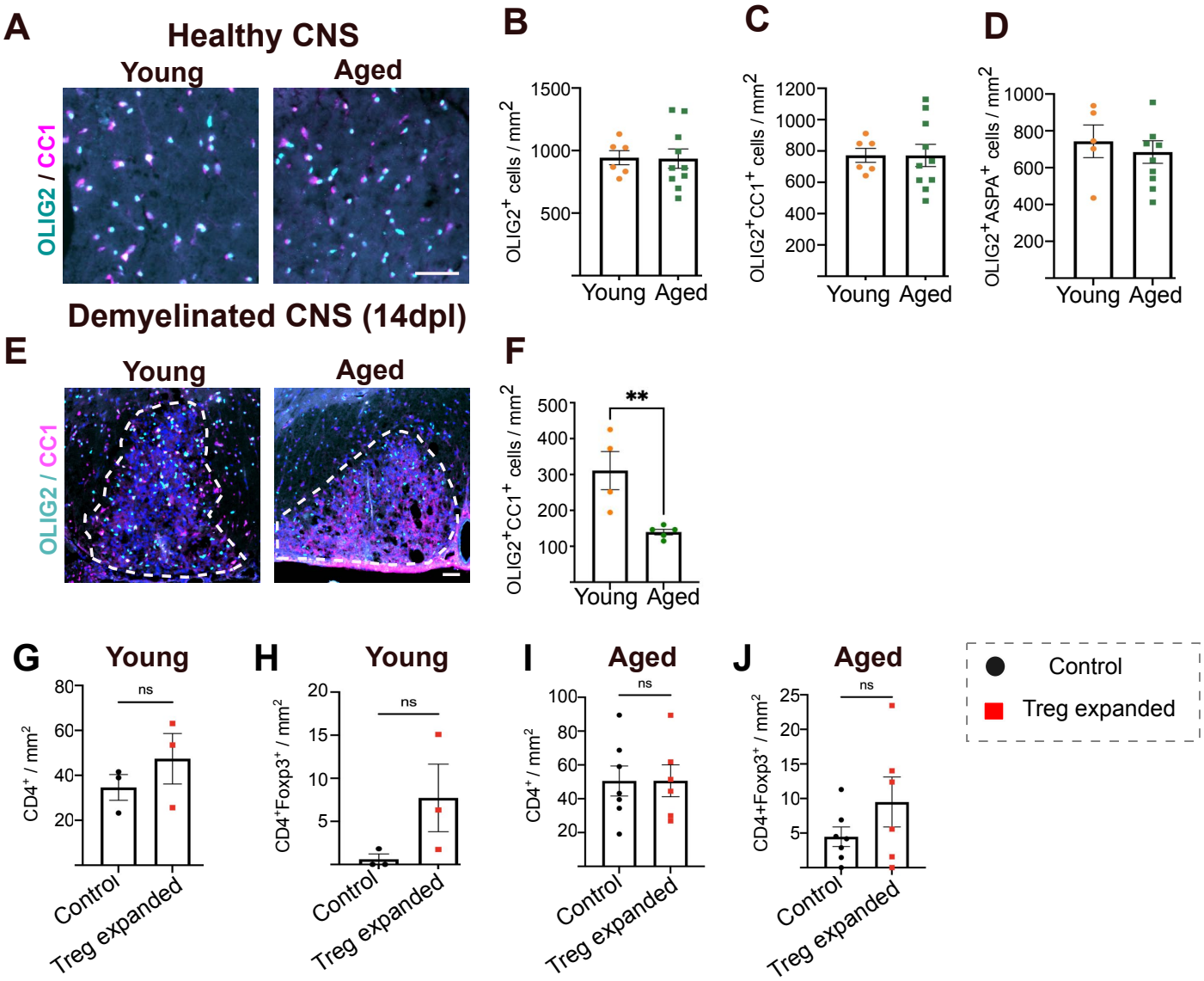
A
Healthy CNS
Young
Aged
OLIG2 / CC1
B
OLIG2+ cells / mm2
1500
1000
500
Young
Aged
C
OLIG2+CC1+ cells / mm2
1200
1000
800
600
400
200
Young
Aged
D
OLIG2+ASPA+ cells / mm2
1000
800
600
400
200
Young
Aged
Demyelinated CNS (14dpl)
E
Young
Aged
OLIG2 / CC1
F
OLIG2+CC1+ cells / mm2
500
400
300
200
100
**
Young
Aged
G
Young
CD4+ / mm2
80
60
40
20
ns
Control
Treg expanded
H
Young
CD4+Foxp3+ / mm2
20
15
10
5
ns
Control
Treg expanded
I
Aged
CD4+ / mm2
100
80
60
40
20
ns
Control
Treg expanded
J
Aged
CD4+Foxp3+ / mm2
25
20
15
10
5
ns
Control
Treg expanded
Control
Treg expanded

Sup. Fig. 2

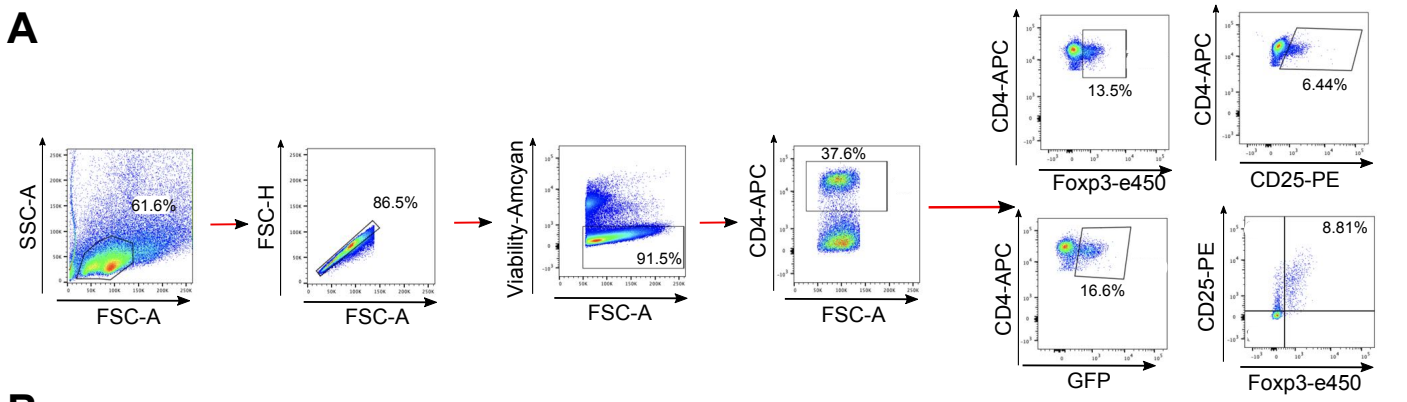
A
SSC-A
FSC-A
61.6%
FSC-H
FSC-A
86.5%
Viability-Amcyan
FSC-A
91.5%
CD4-APC
FSC-A
37.6%
CD4-APC
Foxp3-e450
13.5%
CD4-APC
CD25-PE
6.44%
CD4-APC
GFP
16.6%
CD25-PE
Foxp3-e450
8.81%

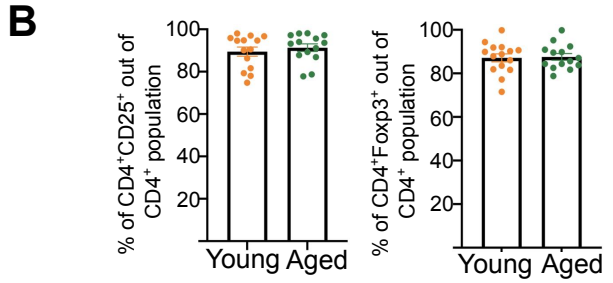
B
% of CD4+CD25+ out of CD4+ population
100
80
60
40
20
Young
Aged
% of CD4+Foxp3+ out of CD4+ population
100
80
60
40
20
Young
Aged

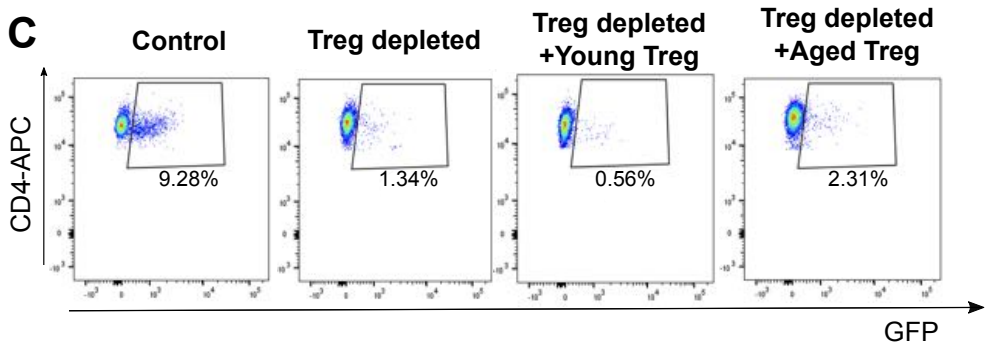
C
Control
Treg depleted
Treg depleted +Young Treg
Treg depleted +Aged Treg
CD4-APC
9.28%
1.34%
0.56%
2.31%
GFP

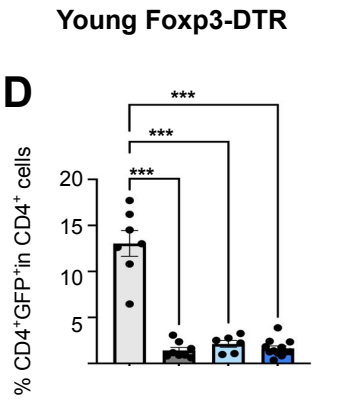
Young Foxp3-DTR
D
% CD4+GFP+in CD4+ cells
20
15
10
5
***
***
***

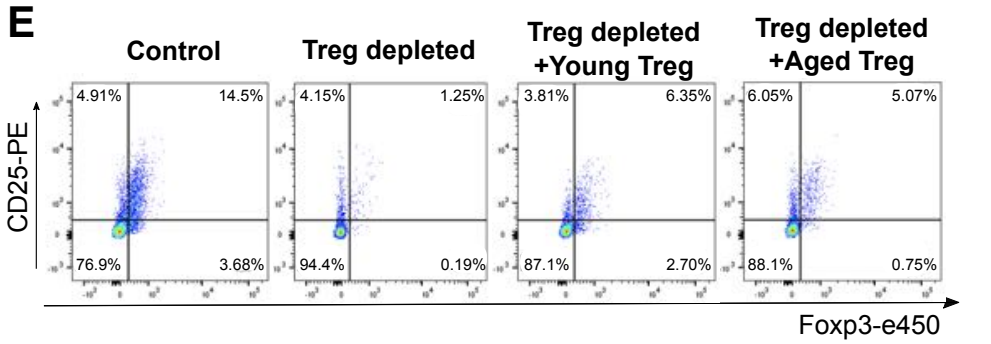
E
Control
Treg depleted
Treg depleted +Young Treg
Treg depleted +Aged Treg
CD25-PE
4.91%
14.5%
76.9%
3.68%
4.15%
1.25%
94.4%
0.19%
3.81%
6.35%
87.1%
2.70%
6.05%
5.07%
88.1%
0.75%
Foxp3-e450

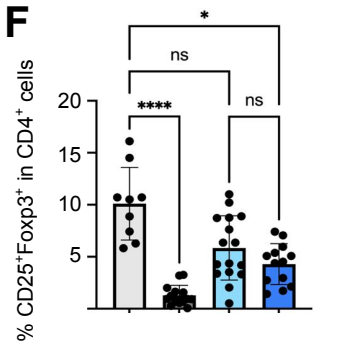
F
% CD25+Foxp3+ in CD4+ cells
20
15
10
5
*
ns
****
ns

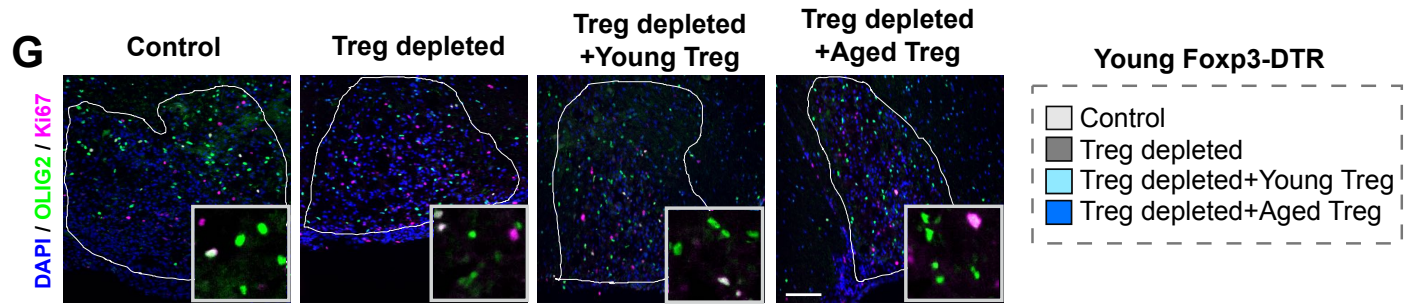
G
Control
Treg depleted
Treg depleted +Young Treg
Treg depleted +Aged Treg
DAPI / OLIG2 / Ki67
Young Foxp3-DTR
Control
Treg depleted
Treg depleted+Young Treg
Treg depleted+Aged Treg

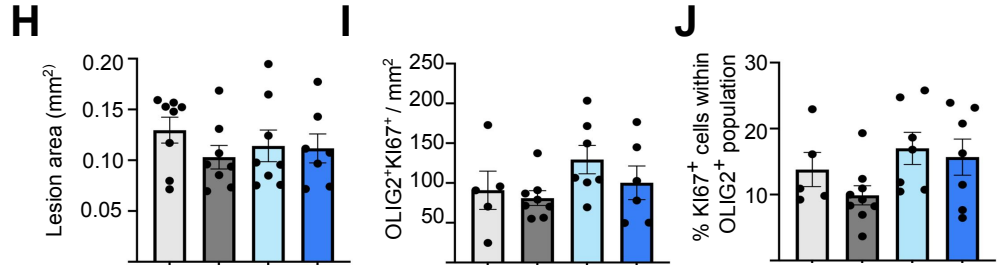
H
Lesion area (mm2)
0.20
0.15
0.10
0.05
I
OLIG2+KI67+ / mm2
250
200
150
100
50
J
% KI67+ cells within OLIG2+ population
30
20
10

Sup. Fig. 3

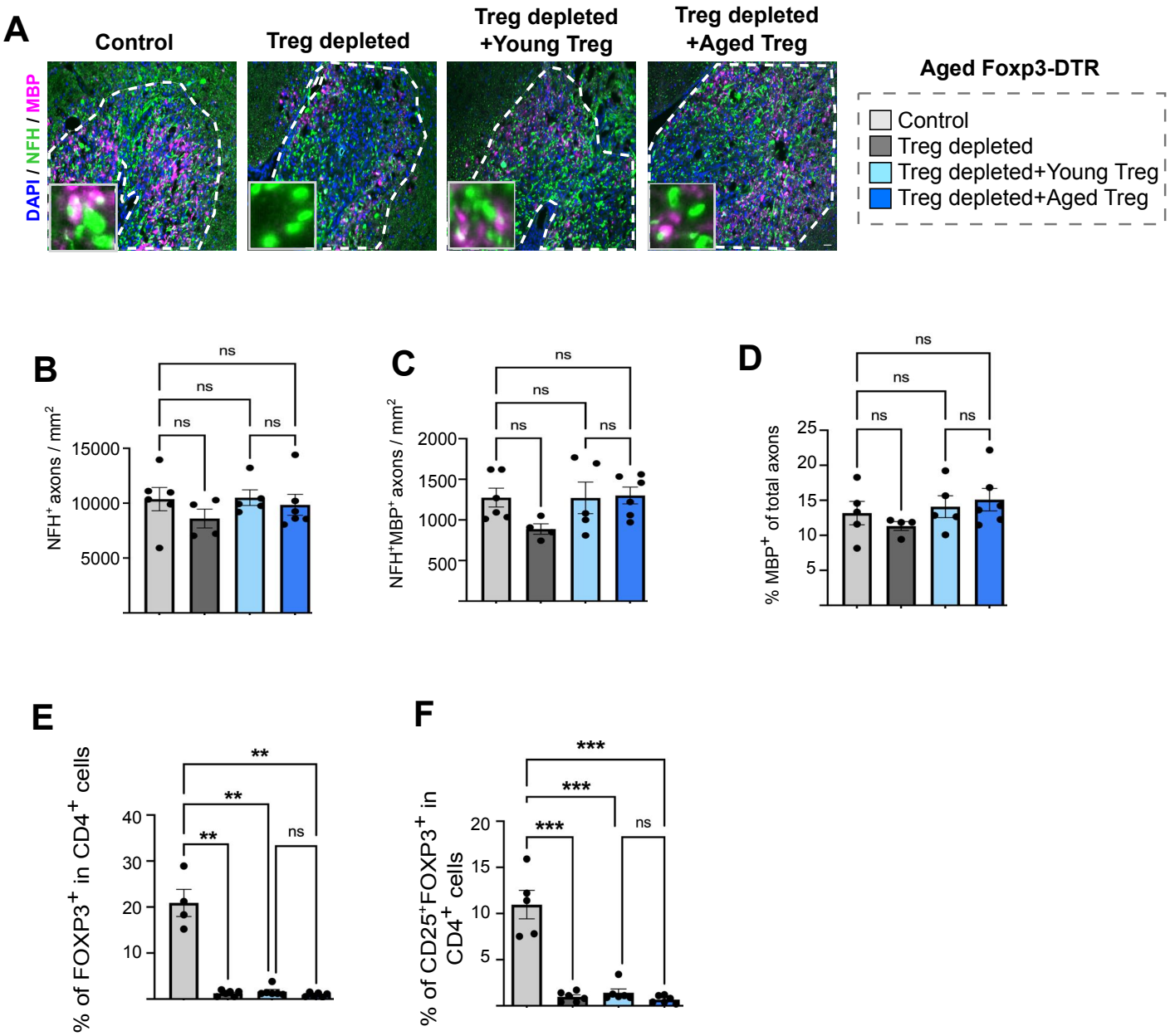
A
Control
Treg depleted
Treg depleted +Young Treg
Treg depleted +Aged Treg
DAPI / NFH / MBP
Aged Foxp3-DTR
Control
Treg depleted
Treg depleted+Young Treg
Treg depleted+Aged Treg
B
NFH+ axons / mm2
15000
10000
5000
ns
C
NFH+MBP+ axons / mm2
2000
1500
1000
500
D
% MBP+ of total axons
25
20
15
10
5
E
% of FOXP3+ in CD4+ cells
40
30
20
10
**
ns
F
% of CD25+FOXP3+ in CD4+ cells
20
15
10
5
***
ns

Sup. Fig. 4

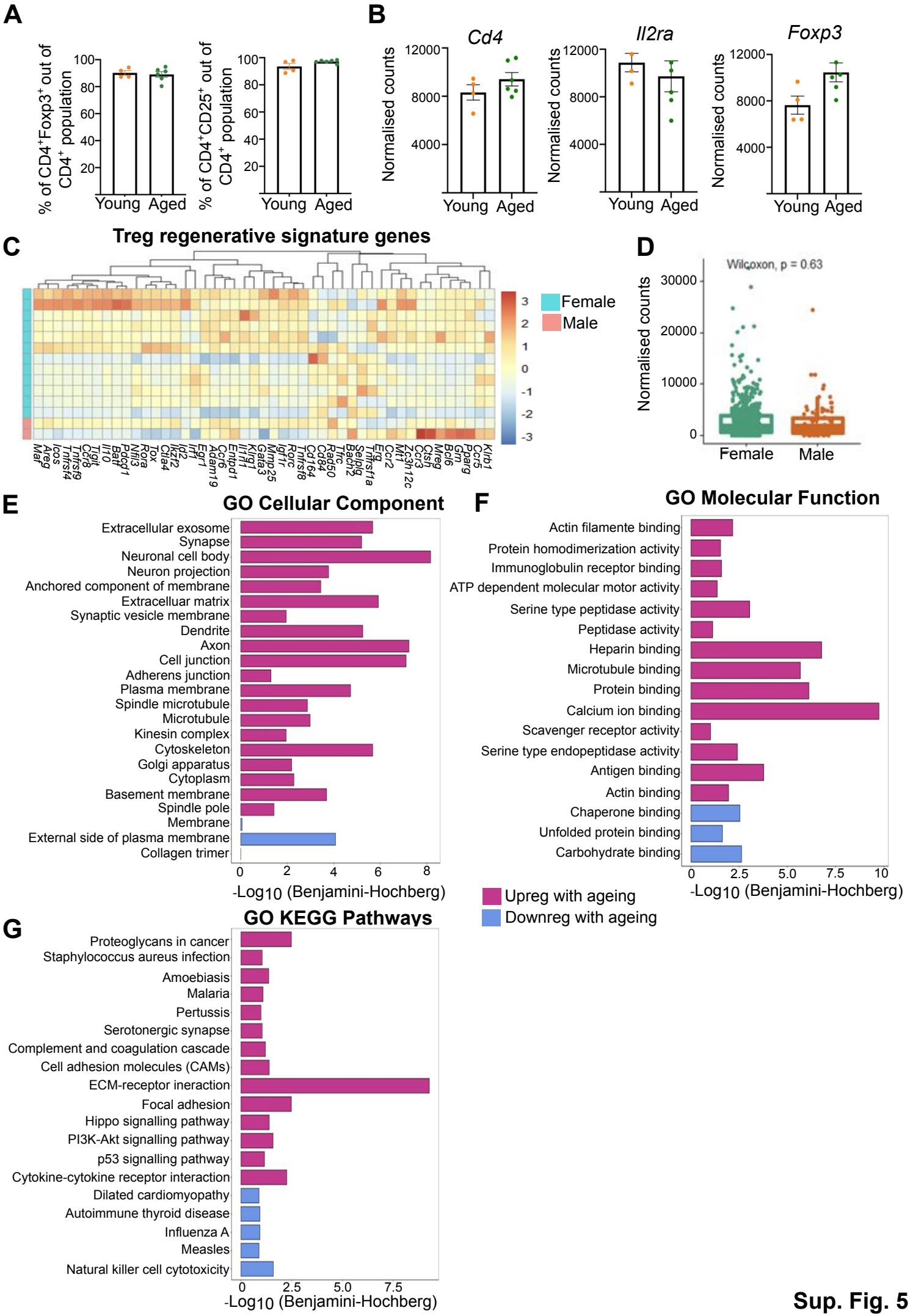
A
% of CD4+Foxp3+ out of CD4+ population
% of CD4+CD25+ out of CD4+ population
Young
Aged
B
Cd4
Il2ra
Foxp3
Normalised counts
C
Treg regenerative signature genes
Female
Male
D
Wilcoxon, p = 0.63
Normalised counts
Female
Male
E
GO Cellular Component
Extracellular exosome
Synapse
Neuronal cell body
Neuron projection
Anchored component of membrane
Extracelluar matrix
Synaptic vesicle membrane
Dendrite
Axon
Cell junction
Adherens junction
Plasma membrane
Spindle microtubule
Microtubule
Kinesin complex
Cytoskeleton
Golgi apparatus
Cytoplasm
Basement membrane
Spindle pole
Membrane
External side of plasma membrane
Collagen trimer
-Log10 (Benjamini-Hochberg)
F
GO Molecular Function
Actin filamente binding
Protein homodimerization activity
Immunoglobulin receptor binding
ATP dependent molecular motor activity
Serine type peptidase activity
Peptidase activity
Heparin binding
Microtubule binding
Protein binding
Calcium ion binding
Scavenger receptor activity
Serine type endopeptidase activity
Antigen binding
Actin binding
Chaperone binding
Unfolded protein binding
Carbohydrate binding
-Log10 (Benjamini-Hochberg)
Upreg with ageing
Downreg with ageing
G
GO KEGG Pathways
Proteoglycans in cancer
Staphylococcus aureus infection
Amoebiasis
Malaria
Pertussis
Serotonergic synapse
Complement and coagulation cascade
Cell adhesion molecules (CAMs)
ECM-receptor ineraction
Focal adhesion
Hippo signalling pathway
PI3K-Akt signalling pathway
p53 signalling pathway
Cytokine-cytokine receptor interaction
Dilated cardiomyopathy
Autoimmune thyroid disease
Influenza A
Measles
Natural killer cell cytotoxicity
-Log10 (Benjamini-Hochberg)

Sup. Fig. 5

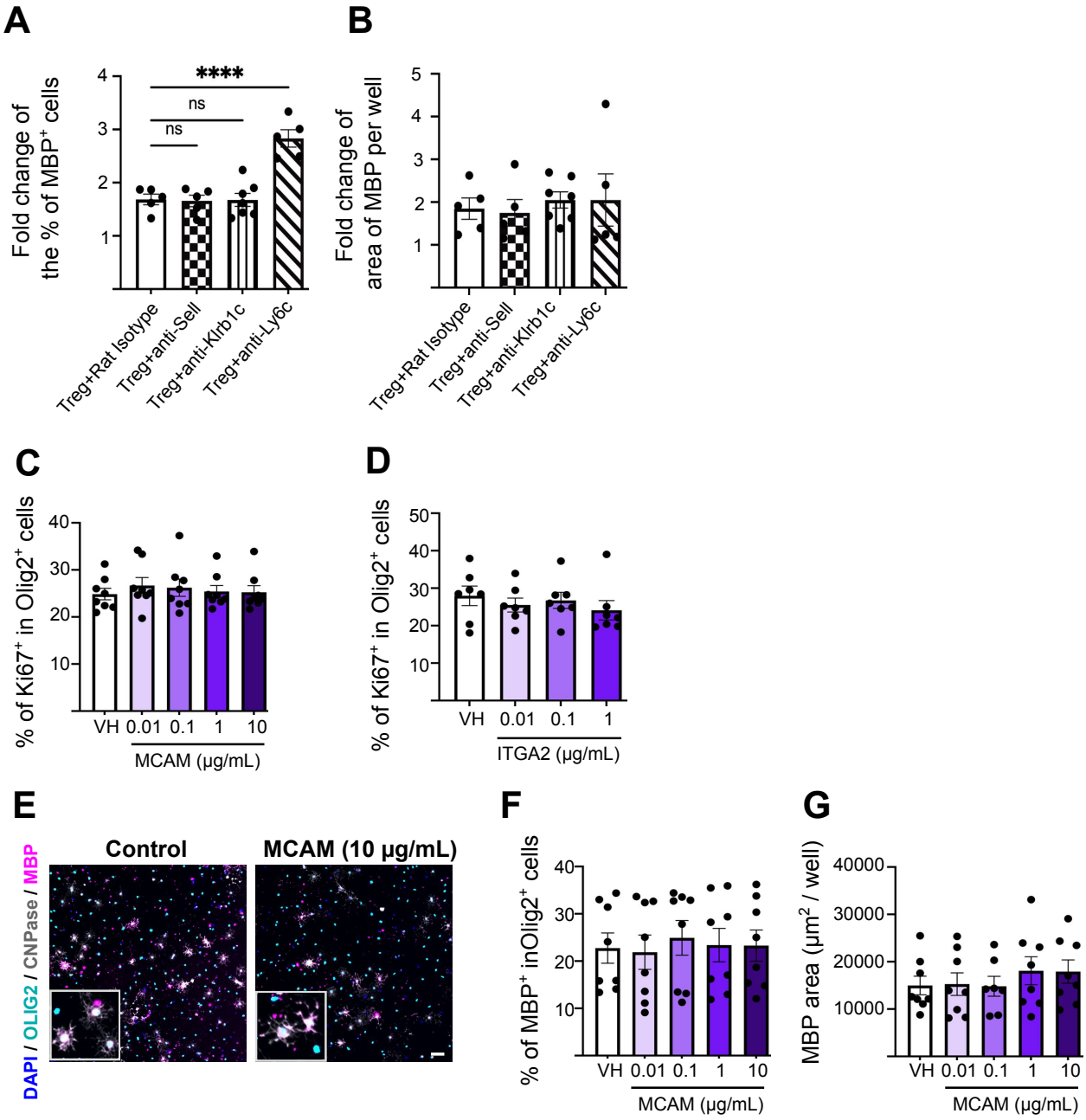
A
Fold change of the % of MBP+ cells
****
ns
ns
Treg+Rat Isotype
Treg+anti-Sell
Treg+anti-Klrb1c
Treg+anti-Ly6c
B
Fold change of area of MBP per well
C
% of Ki67+ in Olig2+ cells
VH 0.01 0.1 1 10
MCAM (µg/mL)
D
% of Ki67+ in Olig2+ cells
VH 0.01 0.1 1
ITGA2 (µg/mL)
E
Control
MCAM (10 µg/mL)
DAPI / OLIG2 / CNPase / MBP
F
% of MBP+ inOlig2+ cells
VH 0.01 0.1 1 10
MCAM (µg/mL)
G
MBP area (µm2 / well)
VH 0.01 0.1 1 10
MCAM (µg/mL)

Sup. Fig. 6

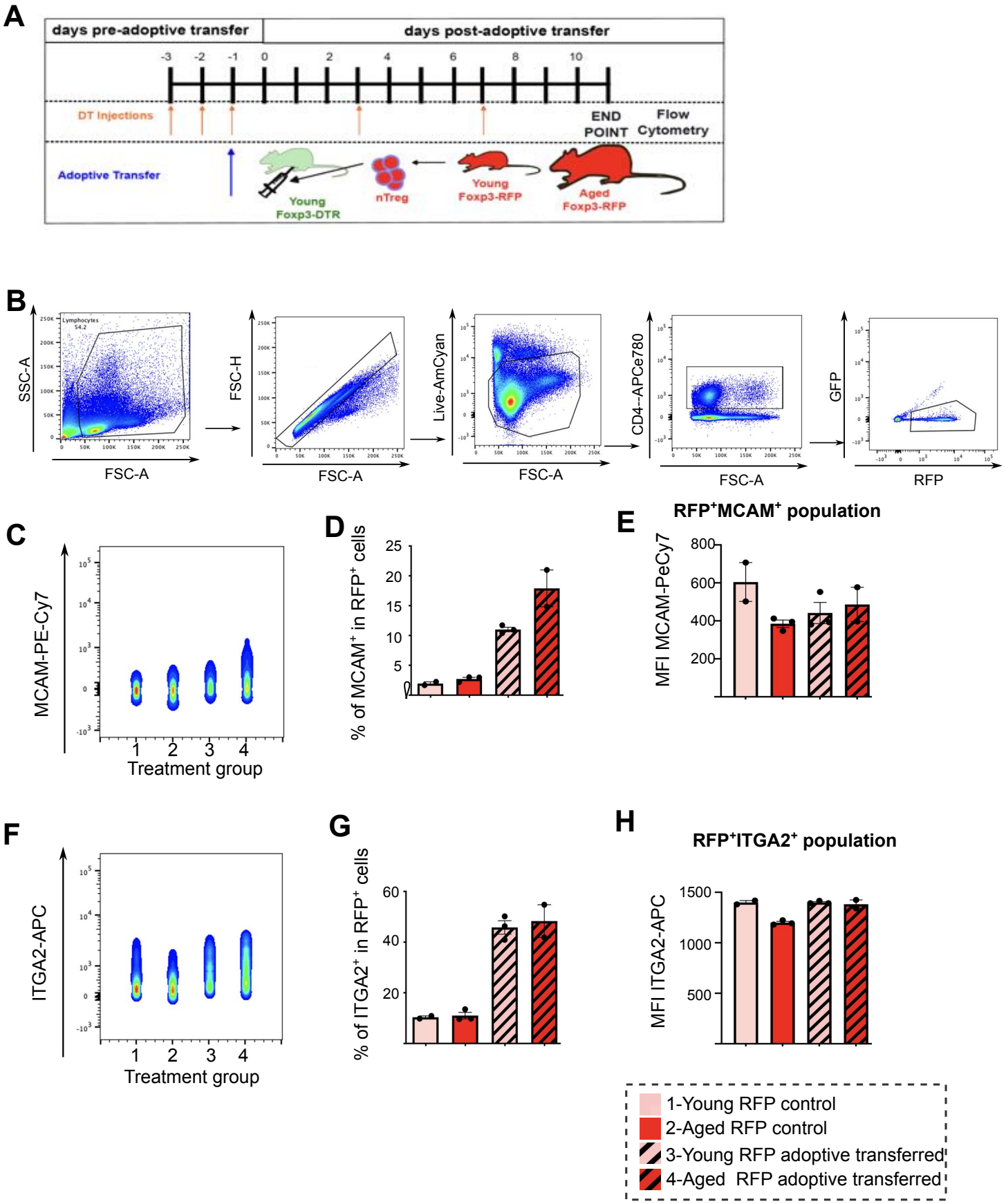
A
days pre-adoptive transfer
days post-adoptive transfer
-3 -2 -1 0 2 4 6 8 10
DT Injections
END POINT
Flow Cytometry
Adoptive Transfer
Young Foxp3-DTR
nTreg
Young Foxp3-RFP
Aged Foxp3-RFP
B
SSC-A
FSC-A
FSC-H
Live-AmCyan
CD4--APCe780
GFP
RFP
C
MCAM-PE-Cy7
Treatment group
D
% of MCAM+ in RFP+ cells
E
RFP+MCAM+ population
MFI MCAM-PeCy7
F
ITGA2-APC
Treatment group
G
% of ITGA2+ in RFP+ cells
H
RFP+ITGA2+ population
MFI ITGA2-APC
1-Young RFP control
2-Aged RFP control
3-Young RFP adoptive transferred
4-Aged RFP adoptive transferred

Sup. Fig. 6